# Absolute oscillator strengths from *K*-shell electron-energy-loss spectra of the fluoroethenes and 1,3-perfluorobutadiene

R. McLaren,* S. A. C. Clark,† I. Ishii, and A. P. Hitchcock‡
*Department of Chemistry, McMaster University, Hamilton, Ontario, Canada L8S 4M1*
(Received 17 February 1987)

Absolute oscillator strengths in the region of carbon and fluorine *K*-shell excitation have been derived for $CH_2CH_2$, $CH_2CHF$, *cis*-CHFCHF, $CH_2CF_2$, $CHFCF_2$, $CF_2CF_2$, 1,3-$C_4H_6$, and 1,3-$C_4F_6$ from electron-energy-loss spectra recorded under dipole-dominated conditions. The methods used to derive absolute oscillator strengths from relative energy-loss intensities are discussed in detail. The accuracy of the procedures is tested through comparisons with literature results for $N_2$, CO, and $CO_2$. The total C $1s\rightarrow\pi^*$ and C $1s\rightarrow\sigma^*$(C—F) intensities increase systematically as the degree of fluorination increases. The spectra are discussed in terms of bond-length correlation and potential barrier concepts.

## I. INTRODUCTION

Inner-shell excitation by electron-energy-loss spectroscopy (ISEELS),[1] photoabsorption,[2] or related techniques such as near-edge x-ray-absorption fine structure (NEXAFS)[3] is a very useful, spatially localized probe of unoccupied electronic structure. In unsaturated molecules such as the fluoroethenes and butadienes, transitions to the $\pi^*$(C=C) and various $\sigma^*$ orbitals are expected to dominate the core excitation spectra. Recently, a correlation between positions of $\sigma^*$ resonances [transitions to quasistationary $(1s^{-1},\sigma^*)$ states] and bond lengths has been demonstrated.[4] This correlation has been a useful guide to the spectral assignments in this work in which we have examined core excitation in 1,3-perfluorobutadiene and the series $C_2H_nF_{4-n}$, $n=0$–4, in order to investigate the effect of fluorination on the virtual valence levels of unsaturated hydrocarbons. Substitution of F for H has been shown to produce a large stabilization in the energies of *occupied* $\sigma$ molecular orbitals (MO's), as determined by photoelectron spectroscopy (PES), while producing relatively small shifts in the $\pi$ energies (the so-called *perfluoro effect*[5]). In a recent study of the core excitation spectra of the fluorobenzenes[6] the energies of the C $1s\rightarrow\pi^*$ transitions were found to increase by only 0.058 eV with each additional fluorine. In contrast, the energies of features assigned to C $1s\rightarrow\sigma^*$(C—F) transitions decreased by approximately 0.24 eV per added fluorine. These observations are consistent with a perfluoro effect on *unoccupied* orbitals.

In the present work we continue to investigate the perfluoro effect on unoccupied orbitals through a study of core excitations to the $\pi^*$ and $\sigma^*$ orbitals of $CH_2CH_2$, $CH_2CHF$, *cis*-CHFCHF, $CH_2CF_2$, $CHFCF_2$, $CF_2CF_2$, $CH_2CHCHCH_2$, and $CF_2CFCFCF_2$. With regard to previous core excitation studies of these species, the carbon 1*s* spectrum of ethene has been studied by both photoabsorption[7] and high-resolution ISEELS.[8,9] The latter was able to resolve vibrational structure in transitions to the (C $1s^{-1},\pi^*$) and various Rydberg states. Detailed *ab initio* calculations of the potential curves, energies, and oscillator strengths for C 1*s* excitation in ethene have been presented by Barth *et al.*[10] The spectra of butenes, 1,3-*trans*-butadiene, and perfluoro-2-butene have been reported[11] as has a high-resolution energy-loss spectrum of 1,3-*trans*-butadiene.[12] Recently, Beckmann *et al.*[13] have reported the parent-ion photoionization yield between 280 and 297 eV for the complete fluoroethene series. Although there are considerable similarities with our results, there are also differences in relative intensities and spectral assignments. The ISEEL or photoabsorption spectra of 1,3-perfluorobutadiene and the fluoroethenes have not been reported previously to our knowledge. ISEEL spectra of a wide range of unsaturated perfluorocarbons (including $F_2CO$, $CF_3C{\equiv}CCF_3$, $CF_3CO_2H$, $(CF_3)_2CO$, and perfluoronaphthalene) have been recorded. These results, which provide further understanding of the perfluoro effect on unoccupied orbitals, are the subject of a forthcoming paper.[14]

Transition intensities as well as energies are useful spectroscopic parameters. Although methods for deriving absolute oscillator strengths from valence-shell electron-energy-loss spectra are well developed,[15] the corresponding procedures for inner-shell excitation have been carried out in only a few cases.[16–18] In this work methods for converting our relative ISEELS intensities to approximate optical oscillator strengths (OS) are described. The accuracy of these procedures is discussed and tested through a comparison of our results for $N_2$, CO, and $CO_2$ with independent measurements reported previously. In cases of well-resolved features such as $1s\rightarrow\pi^*$ transitions, the absolute oscillator strengths allow a detailed investigation of the spatial distribution of the promoted electron in the core excited state. These in turn can be taken as an approximation to that of the virtual orbital in the ground state of the molecule. Absolute oscillator strengths obtained in this fashion have recently been used to map the spatial distribution of the $\pi^*$(C=O) orbital in substituted carbonyls.[19]

In the present work the absolute intensities of the fluoroethene spectra are used to investigate the effects of potential barriers on the $\pi^*$(C=C) and $\sigma^*$(C—F) orbit-

 ©1987 The American Physical Society

als. Potential barrier effects in the core excitation spectra of highly fluorinated molecules have been discussed in detail by Dehmer.[20] In these types of molecules the molecular potential is believed to contain a barrier in the region of the fluorines which divides the molecular potential into an inner- and an outer-well region. In the core excitation spectra of spherically symmetric fluorine cage molecules, the potential barrier is manifested by an increased intensity for transitions between the localized core and unoccupied valence orbitals, which are predominantly located in the inner-well region. Simultaneously, the intensities of transitions to the spatially extended Rydberg orbitals decrease, indicating that these are excluded from the region of the molecular core by the potential barrier. Investigation of the spectra of a related series such as the fluoroethenes allows a clearer investigation of potential barrier effects since the changes in other factors affecting the electronic structure are expected to be minimal. In addition, the highly nonspherical geometry of these molecules might be expected to produce effects different from those predicted by a simple one-dimensional potential barrier model.

When there is more than one chemically distinguishable atom of a single type in a molecule, such as the CHF and $CF_2$ carbons of trifluoroethene, the core excitation spectra contain transitions to the same final level from each distinguishable initial level [denoted as C $1s$(CHF) and C $1s(CF_2)$]. Generally, but not always,[11] the separations of these ISEELS features are similar to the C $1s^{-1}$ chemical shifts as determined by x-ray photoelectron spectroscopy (XPS). The systematic study of a series of similar molecules assists spectral identification; allows an investigation of the influence of the location of the core hole on the term values; and, through comparison of intensities, probes shifts in the spatial distributions of virtual orbitals.

## II. EXPERIMENTAL PROCEDURE

The inner-shell spectra were obtained by inelastic scattering of energetic electrons at $\sim 10^{-4}$ torr sample pressure. The spectrometer was operated under dipole-dominated conditions with a scattering angle of 1°–2° and a final electron energy of 2.5 keV. The spectral resolution was typically 0.6 eV, as measured by the full width at half maximum (FWHM) of the C $1s \rightarrow \pi^*$ transition in CO. More detailed descriptions of the experimental apparatus and techniques of ISEELS have been given elsewhere.[1,11,21] The high-purity gases used in this study were obtained commercially and used without further purification [tetrafluoroethene ($C_2F_4$), trifluoroethene ($CHFCF_2$), and 1,3-perfluorobutadiene ($CF_2CFCFCF_2$) from PCR (Peninsula Chemical Research); ethene, 1,1-difluoroethene ($CH_2CF_2$), and monofluoroethene ($CH_2CHF$) from Matheson]. Sample purity was monitored *in situ* by quadrupole mass spectrometry. The absolute energy scales were determined by calibrating the spectra relative to the C $1s \rightarrow \pi^*$ and O $1s \rightarrow \pi^*$ transitions in CO or $CO_2$ whose absolute energies are known accurately.[22,23]

## III. CONVERSION TO OPTICAL SPECTRA: THEORY AND PROCEDURES

An electron-energy-loss spectrum is a measure of the relative cross section, $d\sigma_n/d\omega$, for excitation of the $n$th excited state by inelastic scattering into the solid angle $\omega$. In the continuum region where the excitation energy is a continuous variable, it is necessary to use $d^2\sigma/d\omega\, dE$, the differential cross section per unit energy range. In the general case[24] it is useful to describe the energy-loss cross section as a function of momentum transfer $\mathbf{K}$ in terms of a differential generalized oscillator strength (GOS), $df(\mathbf{K},E)/dE$, where $\mathbf{K}=\mathbf{k}_0-\mathbf{k}_1$, $\mathbf{k}_0$ and $\mathbf{k}_1$ being the initial and final momenta of the scattered electron. The GOS (given for a discrete transition for simplicity) is related to the measured differential cross section through

$$f(\mathbf{K},E)=(Ek_0/2k_1)(d\sigma/d\omega)\ . \tag{1}$$

In electron-energy-loss spectroscopy at small scattering angles, with impact energies that are large compared to the energy loss, the momentum transfer is small and $f(\mathbf{K},E)$ can be expressed within the Bethe-Born theory as[15,24,25]

$$f(\mathbf{K},E)=f^0(E)+K^2f^1(E)+\cdots\ , \tag{2}$$

where $f^0(E)$ is the optical oscillator strength (determined by the electric dipole matrix element) and $f^1(E)$ contains quadrupole and the product of dipole and octupole matrix elements.

Basically the Bethe-Born treatment[24] relates the scattering intensities in the dipole limit ($K \rightarrow 0$) to optical oscillator strengths through kinematic factors. Ideally, one should measure energy-loss spectra at a range of momentum transfers and extrapolate to $K=0$.[15,18] However, this is difficult to carry out with our apparatus. Instead we *assume* that our experimental spectra are sufficiently dipole dominated so that we can ignore all but the first term in the GOS expansion and thus consider our derived GOS to be identical to the optical OS. Since $K \gtrsim 1$ under our experimental conditions, this can only be true if the dipole matrix element is much larger than the nondipole term [i.e., $f^0(E) \gg f^1(E)$]. Read[26] has argued that this will be generally the case for core excitation since the higher $R$ weighting of the nondipole matrix elements combined with the small spatial extent of the core orbital makes these terms very much smaller than the dipole matrix element. In practice many comparisons of dipole-regime inner-shell energy loss and optical spectra of the same molecule suggest that this approximation is generally valid. According to recent measurements,[18] the oscillator strength of the $1s \rightarrow \pi^*$ transition in $N_2$ decreases by only 13% between the extrapolated optical limit ($K=0$) and the GOS at the momentum transfer of our experiment (2.2 $\text{Å}^{-1}$). However, we note that there are a small number of examples[27–29] where specific nondipole core excitations with small but measureable intensity have been detected in energy-loss spectra recorded under conditions similar to ours.

At $K=0$ the inelastic scattering cross section is related to the optical OS, $f^0$, by[15,24,25]

$$d\sigma/d\omega(0°)=16a_0^2R^2E_0E^{-3}f^0 , \quad (3)$$

where $a_0$ is the Bohr radius, $R$ is the Rydberg constant, $E_0$ is the kinetic energy of the incident electron, and $E$ is the excitation energy. Under these limiting conditions, the shape of an energy-loss spectrum is distorted by a factor of $E^{-3}$ as compared to the corresponding optical spectrum. Because of the nonzero momentum transfer and the finite angular acceptance of the analyzer, the correction for the kinematic factors differs from $E^{-3}$ and a somewhat different formula is required. The conversion that we have chosen to use corrects for a range of finite momentum transfers with the formula[30]

$$f^0_{\rm rel}=(d\sigma/d\omega)_{\rm rel}/\ln(1+\theta_m^2/\theta_E^2) , \quad (4)$$

where $\theta_m=2°$, $\theta_E=E/2E_0$, $E$ is the energy loss, and $E_0=E+2500$ eV. This shape correction factor tilts the data over a typical 50-eV spectral range by 32% in the C 1$s$ and 15% in the F 1$s$ region. Based on comparison with literature optical spectra (see below), this formula was found to be suitable for all energy losses between 200 and 600 eV whereas alternate corrections of the type $E^{-n}$, $2<n<3$, were found to require different parameters at low and high energy losses.

The procedures we have used to convert our relative ISEELS to approximate absolute OS are as follows. First, the underlying valence continuum is removed by subtraction of an extrapolation of a fit of $a(E-b)^c$, $c\sim 4$ to the pre-edge data. Then this is converted to a relative optical spectrum through Eq. (4). The absolute optical oscillator strength scale is then obtained by normalizing either to calculated atomic continuum photoionization oscillator strengths[31] or with a quantum shell Thomas-Reike-Kuhn (TRK)[24] sum-rule constraint. In the simplest form the latter is

$$\sum_n f_n^0+\int_0^\infty [df(\epsilon)/d\epsilon]d\epsilon=N_c , \quad (5)$$

where $N_c$ is the number of core electrons and $\epsilon$ represents energy above the core electron ionization potential (IP). Although small corrections are sometimes applied for the shifts in oscillator strength between subshells because of double excitation or Pauli-forbidden transitions to occupied orbitals, these have been neglected since they are secondary compared to the possible errors in our assumption of the equality of the GOS and the optical OS. For the normalization to calculation,[31] values of 0.77 (C 1$s$), 0.56 (N 1$s$), 0.45 (O 1$s$), and 0.37 (F 1$s$) in units of $10^{-2}$ eV$^{-1}$ were used for the oscillator strength per atom at 25 eV above the experimental IP.

## IV. CONVERSION TO OPTICAL SPECTRA: TESTS OF ACCURACY

In order to investigate the accuracy of our procedures we have recorded the spectra of $N_2$, CO, and $CO_2$ over a very wide energy range (200–1000 eV) and compared literature values with the OS generated by both one-point and sum-rule normalizations. Dehmer and Dill[32] have computed the absolute $K$-shell photoabsorption spectrum of $N_2$ from the first discrete transition up to 100 Ry (1300 eV) above the N 1$s$ IP. When compared to atomic nitrogen, they found that molecular effects were significant only around the core edge. In the case of $N_2$ the molecular bonding results in a replacement of the normal atomic Rydberg structure with an intense $1s\rightarrow\pi^*$ transition below the IP and a $1s\rightarrow\sigma^*$ transition in the continuum.[33] In addition to these near-edge shape resonance effects the core spectra of molecules may differ from those of atoms because of contributions of extended x-ray-absorption fine structure (EXAFS),[30] which is a result of interference between the outgoing electron wave and that part which is scattered back to the core excited atom from surrounding atoms. The period of the modulations is roughly represented by $\sin(2kD)$, where $k=(E/R)^{1/2}/a_0$ is the wave number of the ejected electron and $D$ is the internuclear distance. Extended energy-loss fine structure (EXELFS), the energy-loss counterpart to EXAFS, is also observed in ISEELS (Refs. 34–36) although the intensity of the modulations is generally small in the molecules studied in this work because of the poor electron scattering ability of low-$Z$ atoms.

Above a photoelectron energy of 2 Ry (27 eV) the calculated spectrum of $N_2$ (Ref. 32) is very nearly twice that of atomic nitrogen, with shape resonances or EXAFS modulations becoming less than 1% of the total intensity. This is in accord with the experimental OS of $N_2$ derived by Kay *et al.*[17] from dipole-dominated energy-loss spectra. The agreement with atomic values can be attributed to the fact that for photoelectron energies above 25 eV the kinetic energy of the ejected electron becomes much greater than the molecular potential. The atomic character of the high-energy continuum is the basis of our one-point continuum normalization procedure in which we assume that at a constant energy relative to the IP (chosen for convenience as 25 eV above the IP in this work), the oscillator strength is simply given by the oscillator strength for that type of atom multiplied by the number of such atoms in the molecule.

The $K$-shell OS spectra of $N_2$ and CO derived from both one-point continuum and sum-rule normalizations are shown in Fig. 1 while the C 1$s$ and O 1$s$ spectra of $CO_2$ are presented in Fig. 2. In each case our results are compared to literature optical absorption (or photoionization) results measured directly[37–40] or derived from energy-loss measurements.[17,18] There is reasonable agreement (within 20%) between the results of the two normalization procedures as well as good agreement with the literature results both in terms of the spectral shape and the absolute values. The O 1$s$ photoionization curve for CO obtained by time-of-flight photoemission by Truesdale *et al.*[39] and normalized to the photoabsorption spectrum of Barrus *et al.*[40] is in the worst agreement with our results. However, we note that the statistics of the photoionization measurements are quite poor ($\pm$10%) and that there were severe problems with absorption saturation in the work of Barrus *et al.*[40] Thus we suspect that the poor agreement in this case reflects limitations in the optical measurements rather than problems with our conversion procedure. As an additional check the $1s\rightarrow\pi^*$ oscillator strengths for $N_2$, CO, and $CO_2$ derived from our work are compared to the literature values in Table I. The variation between

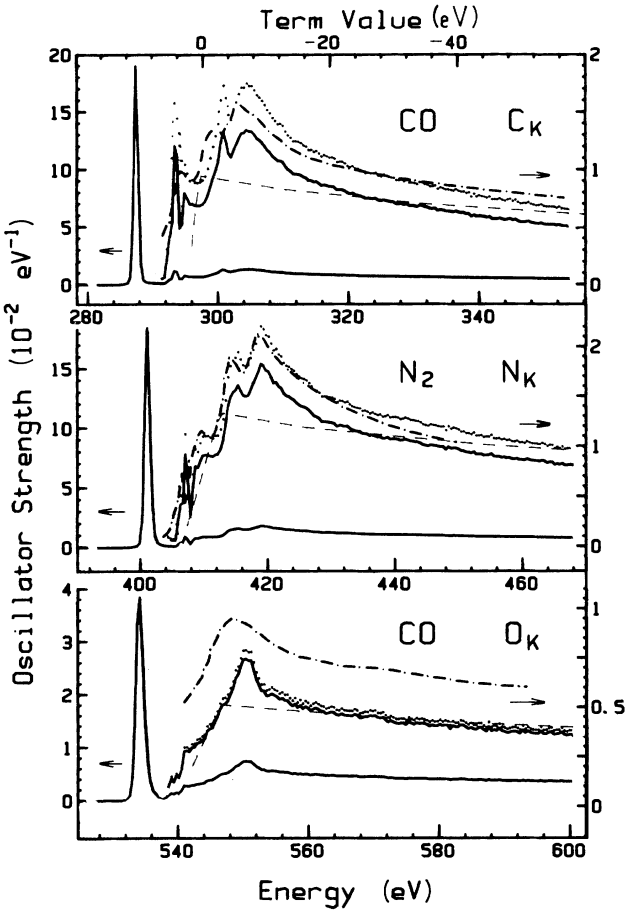


FIG. 1. The oscillator strength spectra of $N_2$ (N 1*s*) and CO (C 1*s* and O 1*s*). ——, derived from dipole-dominated ISEELS using IP + 25 normalization; · · · ·, derived from dipole-dominated ISEELS using sum-rule normalization; — — —, atomic photoionization cross sections (Ref. 31); —·—·—·, experimental literature results: $N_2$, CO-C 1*s* (Ref. 17), CO-O 1*s* (Refs. 39 and 40).

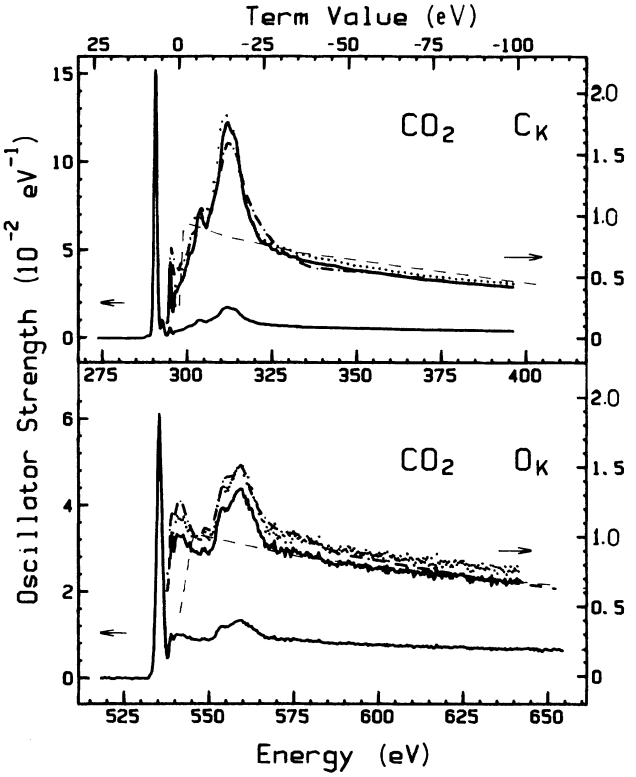


FIG. 2. The oscillator strength spectra of $CO_2$ (C 1*s* and O 1*s*). ——, derived from dipole-dominated ISEELS using IP + 25 normalization; · · · ·, derived from dipole-dominated ISEELS using sum-rule normalization; — — —, atomic photoionization cross sections (Ref. 31); —·—·—·, experimental photoabsorption results (Ref. 38).

our results and the literature values is no worse than that observed among other measurements. Based on these results we are confident that the conversion between the electron and optical shapes is essentially correct and that the one-point continuum or the sum-rule normalization give similar answers within an uncertainty of 20%. For convenience we have used the normalization to calculated atomic oscillator strengths at $E_{IP}$ + 25 eV for the remainder of this work.

One possible systematic error is the effect of potential barriers in highly fluorinated molecules[20] which can depress the near continuum up to 25 eV above the IP. We have tested this with $CF_4$, one of the most extreme cases of potential barrier effects.[41] For the C 1*s* spectrum of $CF_4$ the one-point $\epsilon = 25$ eV normalization gives 20% greater intensity than the sum-rule normalization while the two normalizations differ by less than 10% for the F 1*s* spectrum. Our $CF_4$ results, which will be discussed in full in a subsequent publication,[42] are in good agreement with recent photoabsorption studies.[43] We note here that the C 1*s* spectrum of $CF_4$ differs greatly from that of $CH_4$ in the region of the IP because of the potential barrier effect but the absolute $CH_4$ and $CF_4$ intensities coincide in the continuum at energies higher than 30 eV above the IP and are only 10% different at $\epsilon = 25$ eV. The potential barrier will have the greatest effect on the two perfluoro species of this study, $C_2F_4$ and 1,3-$C_4F_6$, and thus their oscillator strengths may be overestimated through our one-point continuum normalization. However, we argue later that the potential barrier for C 1*s* excitation in these molecules extends only 10–15 eV above the IP so that its effect should be minimal at 25 eV above the IP.

## V. RESULTS AND DISCUSSION

### A. C 1*s* spectra of $C_2H_2$, *cis*-CHFCHF, and $C_2F_4$

In order to interpret the fluoroethene spectra, it is useful to first consider the spectra of $C_2H_4$, *cis*-CHFCHF, and $C_2F_4$ since there is only one carbon environment in each of these species and thus the initial level of each transition is unambiguous.[44] The optical oscillator

TABLE I. $1s \rightarrow \pi^*$ optical oscillator strengths ($f$, units of $10^{-2}$ eV) of $N_2$, CO, and $CO_2$.

| Molecule | core | This work One-point | This work Sum-rule | Literature |
|---|---|---|---|---|
| $N_2$ | N 1s | 18 | 22 | 19(2)[a] 12(5)[b] 22[c] 18[d] |
| CO | C 1s | 15 | 19 | 17(2)[a] |
| CO | O 1s | 5.6 | 5.9 | |
| $CO_2$ | C 1s | 16 | 16 | 14[e] |
| $CO_2$ | O 1s | 12 | 13 | 6.2[e] |

[a]Oscillator strength derived from ISEELS (Ref. 17).
[b]Obtained from Auger intensities using characteristic x-ray emission lines [F. Wuilleumier and M. O. Krause, 1972 International Conference on Inner Shell Ionization, Georgia Inst. of Technology, Atlanta, 1972 (unpublished), p. 773, quoted in Ref. 17].
[c]Direct optical measurement (Ref. 37).
[d]Generalized oscillator strength extrapolated to the optical limit (Ref. 18).
[e]Direct optical measurement (Ref. 38). The $f$ values were measured from the peak areas in Fig. 2 of this reference.

strength spectra in the region of C 1s excitation of $C_2H_4$, *cis*-CHFCHF, and $C_2F_4$ are presented in Fig. 3 on a common term value scale. In order to obtain more accurate energies, to identify overlapping features, and to determine oscillator strengths from peak areas, we have carried out least-squares fittings of the discrete regions of all spectra to Gaussian line shapes. Figure 4 presents an expansion of Fig. 3 in the pre-edge region along with our curve fitting results. The hatched lines in these figures indicate the locations of the IP's as determined directly by XPS (Ref. 45) or estimated in the case of *cis*-CHFCHF. The energies, term values ($T = E_{IP} - E$), and proposed assignments for the C 1s spectral features are listed in Table II.

The first feature in the C 1s spectrum of each species is clearly the C $1s \rightarrow \pi^*(C{=}C)$ transition. As with the spectra of most other unsaturated species, it is the most intense ISEELS feature. Although the absolute energies of the $1s \rightarrow \pi^*$ transitions shift by 5.4 eV from $C_2H_4$ to $C_2F_4$, almost all of this shift arises from changes in the C 1s orbital energies since the C 1s IP shifts by 5.7 eV from $C_2H_4$ to $C_2F_4$ according to XPS.[45] The trends in the C $1s \rightarrow \pi^*$ term values are discussed in detail in Sec. V F.

The second band in the C 1s spectrum of both *cis*-CHFCHF and $C_2F_4$ is relatively intense and in each case is composed of two components. Based on the term values [4.6 eV (*cis*-CHFCHF) and 4.8 eV ($C_2F_4$), derived from curve fitting (see Fig. 4)] and the bond-length correlation,[4] we assign the more intense, lower energy component of this feature to C $1s \rightarrow \sigma^*(C{-}F)$ transitions. Corresponding $\sigma^*(C{-}F)$ features can be identified in

TABLE II. Absolute energies ($E$, eV), term values ($T$, eV), and proposed assignments for features in the C 1s spectra of $CH_2{=}CH_2$, *cis*-CHF=CHF, and $CF_2{=}CF_2$.

| | $CH_2{=}CH_2$ | | *cis*-CHF=CHF | | | $CF_2{=}CF_2$ | | | Proposed | Parent ion yield (Ref. 13) | | |
|---|---|---|---|---|---|---|---|---|---|---|---|---|
| No.[a] | $E$ | $T$[b] | No. | $E$ | $T$ | No. | $E$ | $T$ | assignment | CHFCHF | $C_2F_4$ | assignment |
| 1 | 284.7[c] | 6.1 | 1 | 287.3[c] | 6.4 | 1 | 290.1[c] | 6.4 | $\pi^*$ | 287.8 | 290.1 | $\pi^*$ |
| | | | 2 | 289.1 | 4.6 | 2 | 291.8 | 4.8 | $\sigma^*(C{-}F)$ | 289.8 | 291.9 | 3s |
| 2 | 287.4 | 3.4 | 3 | 290.1 | 3.6 | 3 | 292.5 | 4.0 | 3s | | | |
| 3 | 287.8 | 3.0 | 4 | 291.2 | 2.5 | 4 | 294.4 | 2.1 | 3p | | | |
| 4 | 289.3 | 1.5 | | | | | | | 4p | | | |
| | | | 5 | 293.6 | 0.1 | 5 | 296.5 | 0.1 | Higher Ryd, continuum onset | | | |
| IP | 290.8[d] | | IP | 293.7[e] | | IP | 296.54[d] | | | | | |
| 5 | 292.6 | −1.8 | 6 | 295.4 | −1.7 | 6 | 298.4 | −1.9 | ?-1[f] | | | |
| 6 | 295.8 | −5.0 | 7 | 298.3 | −4.6 | 7 | 302.0 | −5.5 | ?-2[f] | | | |
| 7 | 301(2) | −10 | 8 | 301(2) | −7 | 8 | 310(1) | −13 | $\sigma^*(C{=}C)$ | | | |

[a]Note that the numbering refers to Figs. 3 and 4 and differs from that in other work (Refs. 8 and 9). The numbers are for convenience of cross referencing only.
[b]$T = E_{IP} - E$.
[c]Calibration: $C_2H_4$ (from Ref. 8); CHF=CHF (located 3.49 eV below (C $1s^{-1}, \pi^*$) in $CO_2$ [290.74 eV (Ref. 23)]); $C_2F_4$ (located 2.73 eV above (C $1s^{-1}, \pi^*$) in CO [287.40 eV (Ref. 22)]).
[d]From XPS (Ref. 45).
[e]Estimated as the average of C 1s(CHF) of $CH_2CHF$ (293.48) and $CHFCF_2$ (293.87) (Ref. 45).
[f]Assignment unclear, see text.

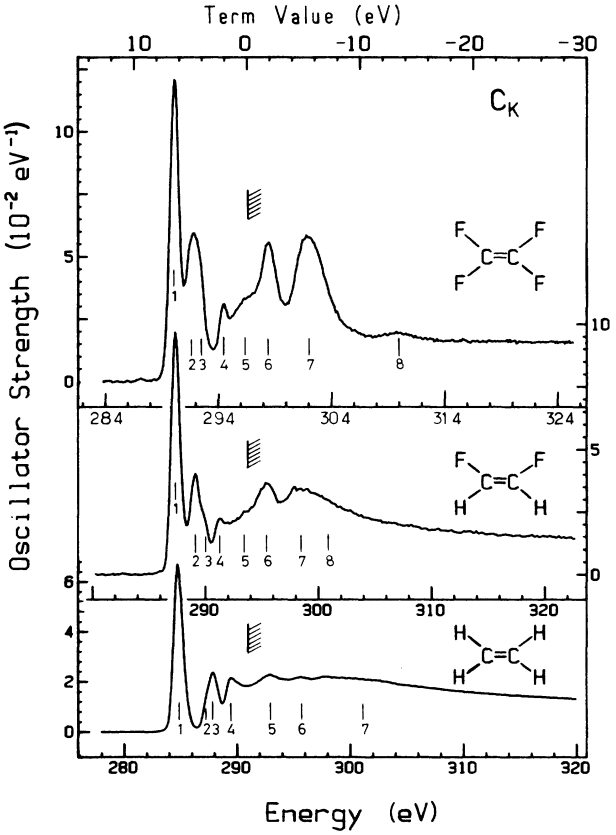


FIG. 3. Absolute oscillator strengths of $C_2H_4$, *cis*-CHFCHF, and $C_2F_4$ in the region of C 1*s* excitation, derived (using IP + 25 eV normalization) from electron-energy-loss spectra recorded with 2.5-keV final electron energy, 2° scattering angle, and 0.6-eV FWHM resolution. The hatched lines indicate the XPS IP's. The energy scales are shifted so as to plot the spectra on the constant term value scale given at the top of the figure.

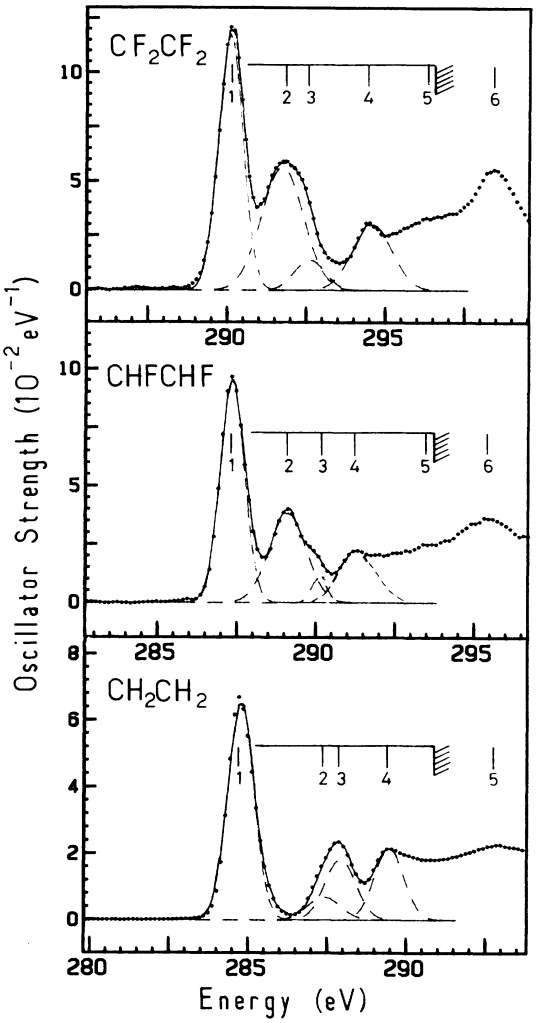


FIG. 4. Expansions of the spectra presented in Fig. 3 in the region below the C 1*s* IP's. Points are the transformed, recorded data; dashed lines are the fitted Gaussians; the solid curve is the sum of the fitted curves.

the C 1*s* spectra of all fluoroethenes (see Sec. V B), although in several cases they are obscured by core-level-shifted C $1s \rightarrow \pi^*$ transitions and are best visualized by the curve fitting results (Figs. 4 and 6). There is a relatively strong band in $C_2H_4$ at 288 eV (features 2 and 3) which superficially resembles the second band of *cis*-CHFCHF and $C_2F_4$. However, the term value in $C_2H_4$ is considerably lower. The high-resolution C 1*s* spectrum of $C_2H_4$ (Ref. 9) shows that this feature is actually a superposition of six or seven peaks which correspond to the vibrational substructure of C $1s \rightarrow 3s$ and C $1s \rightarrow 3p$ transitions. The latter may have some $\sigma^*$(CH) valence character as well since a polarization-dependent band is observed at the same energy in the NEXAFS spectrum of condensed ethene.[46,47] Thus we believe the superficial resemblance of the spectra of $C_2H_4$ and the fluoroethenes in this region is largely an accident of our limited resolution. The high-energy shoulders (No. 3) of the second band of *cis*-CHFCHF and $C_2F_4$ are attributed to C $1s \rightarrow 3s$ Rydberg transitions corresponding to feature 2 in $C_2H_4$. The coexistence in $CH_3F$ of two states around the same energy, one predominantly C $1s \rightarrow \sigma^*$(C—F) valence and the other predominantly C $1s \rightarrow 3s$ Rydberg in character, has been a source of considerable discussion.[48,49] Since these configurations have the same symmetry in $CH_3F$, each state is probably a mixture of both configurations. Mixing of $(1s^{-1}, 3s)$ and $(1s^{-1}, \sigma^*(\text{C—F}))$ configurations may also be important in the fluoroethenes.

Several other weak features are observed between the $\sigma^*$(C—F) transition and the ionization threshold in the C 1*s* spectra of *cis*-CHFCHF and $C_2F_4$. We assign these to C $1s \rightarrow np$ Rydberg transitions as outlined in Table II. According to the potential barrier model of the core excitation spectra of highly fluorinated molecules,[20] core→Rydberg transitions will be very weak if the Rydberg orbitals are excluded from the region of the core by the potential barrier. We observe that the intensities of features 3 (3*s*), 4 (3*p*), and 5 (higher Rydberg) are similar to those of features 2–4 in the C 1*s* spectrum of $C_2H_4$

with possibly stronger $1s \rightarrow 3s$ and weaker $1s \rightarrow np$ transitions in the more fluorinated species. This suggests that the potential barrier is anisotropic as in planar $BF_3$ and is sufficiently weak perpendicular to the molecular plane to allow appreciable intensity for transitions to the roughly spherically symmetric Rydberg orbitals. Barth *et al.*[10] have calculated oscillator strengths for the $1s \rightarrow \pi^*$ (0.088), $3s$ (0.003), and $3p$ (0.004) transitions in ethene. Their $\pi^*$ value is similar to the OS we obtain (0.068) but the calculated OS for the Rydberg transitions are 3 to 5 times smaller than our values ($3s$ (0.009), $3p$ (0.022)). The higher experimental intensity may be considered as supporting evidence for a partial $\sigma^*$(C—H) character for these transitions in $C_2H_4$.

The weak but well-defined feature (No. 8) high in the C $1s$ continuum of $C_2F_4$ ($T=13$ eV) appears to correspond to the broad maximum (No. 7) in the C $1s$ spectrum of $C_2H_4$ ($T=11$ eV) which has been assigned to C $1s \rightarrow \sigma^*$(C=C) transitions, i.e., the $\sigma^*$(C=C) shape resonance.[4] The positions of the $\sigma^*$(C=C) shape resonances predicted from the empirical bond-length correlation[4] are 13.3 eV for $C_2F_4$, 12.7 eV for *cis*-CHFCHF, and 11.8 eV for $C_2H_4$ (see Table VIII and Sec. V I for further discussion of the bond length and $\sigma^*$ resonance data). These values are in good agreement with those of feature 8 in $C_2F_4$ and feature 7 in $C_2H_4$. Surprisingly we do not observe a feature at the corresponding energy in *cis*-CHFCHF although the $\sigma^*$(C=C) resonance may be No. 8, the broad high-energy shoulder of No. 7 since No. 7 is much broader than its counterpart in $C_2F_4$. A polarization-dependent continuum feature has recently been observed at similar energies in the NEXAFS spectra of multilayer and monolayer $C_2H_4$ on Cu(100) (Ref. 46) and Ag(100) (Ref. 47). The observed polarization dependence is consistent with a $\sigma^*$(C=C) assignment if the C—C axis of the chemisorbed ethene is parallel to the Cu or Ag surface. The $\sigma^*$(C=C) energies in the spectra of the surface species are somewhat smaller than those for gas phase $C_2H_4$. This was interpreted in terms of lengthening of the C=C bond as the ethene bonds to the metal surface. Both the polarization behavior, and the fact that the peak is closer to the gas-phase value on the less reactive silver surface[47] than on the more reactive Cu (Ref. 46) or Pt (Ref. 3) surfaces, are very supportive of the $\sigma^*$(C=C) assignment.

Features 6 and 7 in the C $1s$ continuum of *cis*-CHFCHF and $C_2F_4$ are rather puzzling. In Table II they have been labelled ?-1 and ?-2 to reflect our uncertainty as to their assignment. Based on their term values and shape, they seem to be intensity-enhanced versions of features 5 and 6 in $C_2H_4$. This connection can be traced throughout the fluoroethene series as indicated by the (?-1,?-2) assignments in Tables II and III. They could be attributed to $\sigma^*$(C=C) transitions split by interaction with other $\sigma^*$ orbitals such as $\sigma^*$(C—H) or $\sigma^*$(C—F). However, we prefer to assign feature 7 in $C_2H_4$ exclusively to the $1s \rightarrow \sigma^*$(C=C) transition. The features corresponding to No. 5 and No. 6 in the C $1s$ spectrum of surface adsorbed $C_2H_4$ are very weak and have a weak $\pi$ polarization, if any at all,[46,47] contrary to that expected for a C $1s \rightarrow \sigma^*$(C=C) transition in a molecule oriented with its C=C bond parallel to the surface. Features 6 and 7 in *cis*-CHFCHF and $C_2F_4$ are possibly additional C $1s \rightarrow \sigma^*$(C—F) transitions. The four unoccupied $\sigma^*$ (C—F) levels of $C_2F_4$ given by a minimal basis set could be assigned to features 2, 6, and 7. An argument against this interpretation is that the continuity between features 6 and 7 in *cis*-CHFCHF and $C_2F_4$ and features 5 and 6 in $C_2H_4$ would seem unlikely if the transitions really are to $\sigma^*$(C—F) orbitals.

In earlier experimental[8] and theoretical[10] studies of $C_2H_4$, features 5 and 6 were attributed to double excitations (probably simultaneous $1s \rightarrow \pi^*$ and $\pi \rightarrow \pi^*$ transitions). The intensities of the corresponding features (Nos. 6 and 7) in $C_2F_4$ seem to be too large for this interpretation. Another interesting aspect of ?-1 and ?-2 is the intensity of corresponding features in the F $1s$ spectra (see Fig. 9 and Sec. V E). Assignments based on term value comparison suggest that the F $1s \rightarrow$?-2 transitions are relatively strong features while the F $1s \rightarrow$?-1 transitions are very weak. This suggests that, if these are one-electron excitations, as seems likely from their intensity in the C $1s$ spectrum of $C_2F_4$, the ?-1 orbital is localized on the carbons while the ?-2 orbital has appreciable density on both C and F. Calculations of the one-electron and multielectron C $1s$ excitation and ionization spectra, along with the C $1s$ spectrum of oriented $C_2F_4$, would be of great assistance in deducing the correct interpretation of these two features.

It is possible that all continuum features in these molecules are one-electron transitions to orbitals with at least some $\sigma^*$(C=C) character. This is believed to be the situation in benzene, pyridine,[50,51] and in the fluorobenzenes.[6] If all three of these features are one-electron transitions to $\sigma^*$ orbitals, the discrepancy between the positions of the lower-energy continuum features and the bond-length correlation[4] can be understood in terms of mixing of adjacent $\sigma^*$(C=C), $\sigma^*$(C—H), and $\sigma^*$(C—F) levels and thus loss of the localized character of the $\sigma$ resonances. From the values predicted by the bond-length correlation, feature 8 of $C_2F_4$ and feature 7 of $C_2H_4$ are interpreted as the dominant $1s \rightarrow \sigma^*$(C=C) transitions. It is interesting to note that there is negligible change in the intensity of this high-energy feature with fluorination. At first inspection this seems inconsistent with the potential barrier model[20] since the $\sigma^*$(C=C) orbital might be expected to be inner well and thus enhanced upon fluorination. The apparent enhancement of the ?-1 and ?-2 transitions at approximately 2 and 6 eV above the IP but not that of the $\sigma^*$(C=C) at approximately 12 eV above the IP can be interpreted either in terms of an effective barrier height for C $1s$ excitation in the fluoroethenes around 8 eV or as an effect of barrier anisotropy.

### B. C 1s spectra of CHF=CH$_2$, CH$_2$=CF$_2$, and CHF=CF$_2$

The C $1s$ spectra of $CHFCH_2$, $CH_2CF_2$, and $CHCF_2$, which each have two distinguishable carbon environments, are presented in Fig. 5 on an absolute energy scale. Expansions of the discrete region and our curve fitting interpretation are given in Fig. 6 while the ener-

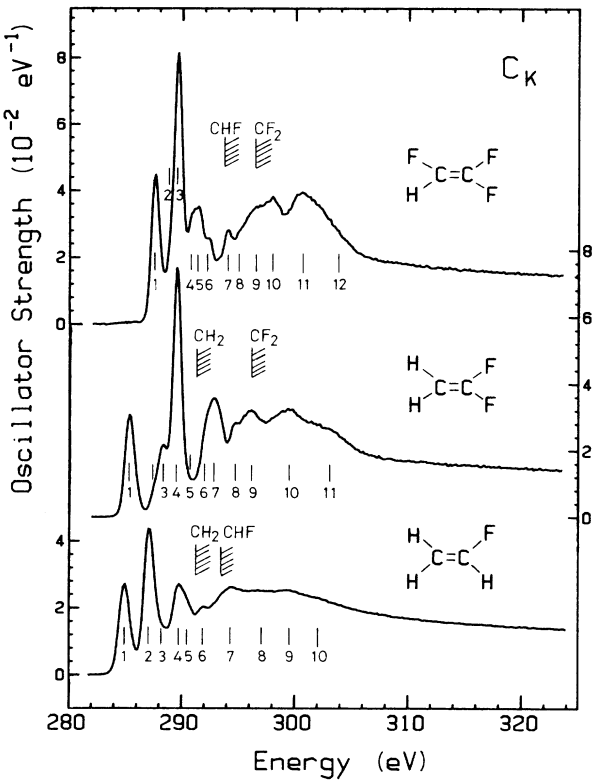


FIG. 5. Absolute oscillator strengths of $CHFCH_2$, $CF_2CF_2$, and $CHFCF_2$ in the region of C 1$s$ excitation. See Fig. 3 caption for further details.

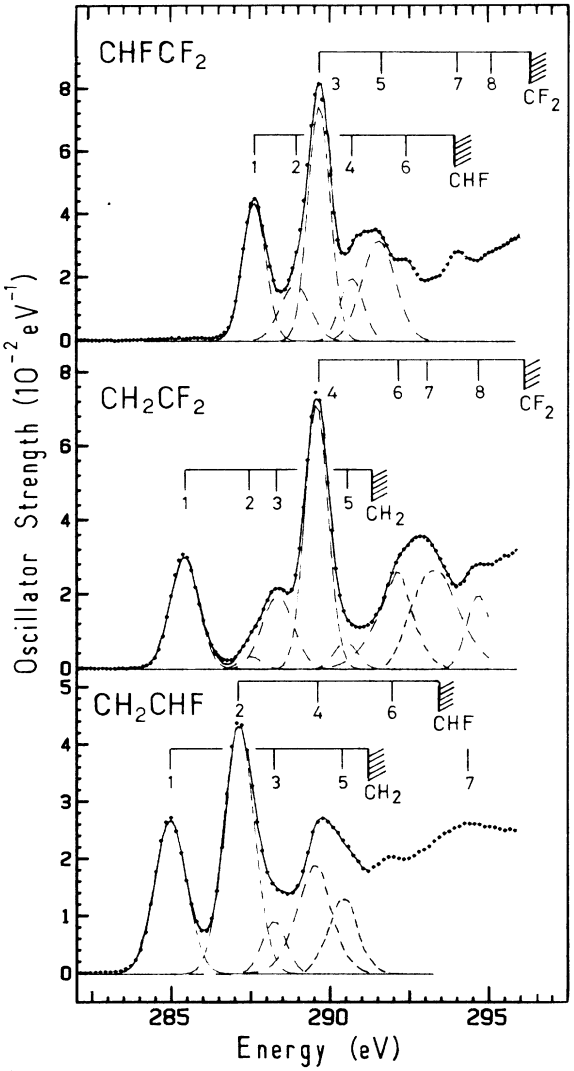


FIG. 6. Expansions of the spectra presented in Fig. 5 in the region below the C 1$s$ IP's. Points and dashed and solid lines as in Fig. 4.

gies, term values, and proposed assignments are listed in Table III. The assignments of the features observed in the C 1$s$ spectra of these molecules follow from those of $C_2H_4$, *cis*-CHFCHF, and $C_2F_4$ in the sense that these spectra are considered representative of C 1$s$($CH_2$), C 1$s$(CHF), and C 1$s$($CF_2$) excitations. The C 1$s$ spectra of the intermediate fluoroethenes are interpreted as the superposition of transitions from two chemically distinguishable carbon 1$s$ orbitals to a common manifold of unoccupied orbitals. The C $1s \rightarrow \pi^*$ transitions in each of the intermediate fluoroethenes are easily identified as the intense, sharp features at lower energy on the basis of their term values relative to the appropriate C 1$s$ IP. The term values and oscillator strengths of the $\pi^*$(C=C) features in all of the fluoroethenes are summarized in Table V. Discussion of the trends in these quantities is postponed until Secs. V F and V G.

Paddon-Row *et al.*[52] have calculated the ground-state geometries of the $\pi^*$ radical anions of $C_2H_4$, $CH_2CHF$, $CH_2CF_2$, and $C_2F_4$. They have concluded that the addition of one electron to the $\pi^*$ orbital causes each of these molecules to adopt a chairlike, nonplanar *anti*-structure with the degree of nonplanarity increasing with the degree of fluorination. One might expect that the (C $1s^{-1}$,$\pi^*$) state will have an equilibrium geometry similar to that of the $\pi^*$ radical anion, which suggests that extensive excitation of the out-of-plane bending vibrational mode may occur. This could result in systematic changes in the widths of the C $1s \rightarrow \pi^*$ transitions. However, these widths are very similar: 1.0±0.1 eV in all of the fluoroethenes. Since this is significantly greater than our experimental resolution (0.6 eV), this is not necessarily inconsistent with the postulated nonplanar geometry of the $\pi^*$ excited state. High-resolution ISEELS shows that the $\nu_{C-H}$ stretch mode is extensively excited in the C $1s \rightarrow \pi^*$ transition of $C_2H_4$.[8-10] In contrast, in the C 1$s$ spectrum of $CHFCH_2$ obtained at comparable high resolution,[53] the two C $1s \rightarrow \pi^*$ transitions have similar widths to the C $1s \rightarrow \pi^*$ feature of $C_2H_4$ but the $\nu_{C-H}$ stretch mode is not clearly resolved. The broadened vibronic lines in $CHFCH_2$ suggest that an additional mode, possibly the out-of-plane bending mode, is simultaneously excited. Based on their calculations of the (C $1s^{-1}$, $\pi^*$) potential curves of $C_2H_4$, Barth *et al.*[10] have concluded that, although the equilibrium geometry

TABLE III. Absolute energies, term values, and proposed assignments for the C 1*s* spectra of $CH_2CHF$, $CH_2CF_2$, and $CHFCF_2$.

$CH_2CHF$

| | | | | | | Parent ion yield (Ref. 13) | | |
|---|---|---|---|---|---|---|---|---|
| | *E* | *T* (eV) | | Assignment | | *E* | Assignment | |
| No. | (±0.2 eV) | $CH_2$ | CHF | $CH_2$ | CHF | (±0.6 eV) | CHF | $CF_2$ |
| 1 | 285.0[a] | 6.1 | | $\pi^*$(C—C) | | 284.6 | $\pi^*$ | |
| 2 | 287.1 | | 6.4 | | $\pi^*$(C—C) | 286.9 | 3*s* | $\pi^*$ |
| 3 | 288.3[b] | 2.8 | | 3*p* | | | | |
| 4 | 289.7 | 1.4 | 3.8 | Ryd | $\sigma^*$(C—F) | 288.8 | 3*d* | |
| 5 | 290.4 | 0.7 | 1.6 | Ryd | Ryd | | | |
| IP[c] | 291.10($CH_2$) | | | | | | | |
| 6 | 291.9 | | 1.6 | | Ryd | 292.2 | | 4*p* |
| IP[c] | 293.48(CHF) | | | | | | | |
| 7 | 294.4 | −3.3 | | ?-1 | | 293.8 | | ? |
| 8 | 296.8(3) | | −3.3 | | ?-1 | | | |
| 9 | 299.3(3) | −8.2 | | ?-2 | | | | |
| 10 | 302.3(5) | −11.2 | −8.8 | $\sigma^*$(C=C) | ?-2 | | | |

$CH_2CF_2$

| | | | | | | Parent ion yield (Ref. 13) | | |
|---|---|---|---|---|---|---|---|---|
| | *E* | *T* (eV) | | Assignment | | *E* | Assignment | |
| No. | (±0.2 eV) | $CH_2$ | $CF_2$ | $CH_2$ | $CF_2$ | (±0.6 eV) | CHF | $CF_2$ |
| 1 | 285.4 | 5.9 | | $\pi^*$(C—C) | | 284.9 | $\pi^*$ | |
| 2 | 287.5 | 3.8 | | 3*s* | | 287.7 | 3*s* | |
| 3 | 288.4 | 3.0 | | 3*p* | | | | |
| 4 | 289.6[a] | | 6.5 | | $\pi^*$(C—C) | 289.2 | | $\pi^*$ |
| 5 | 290.5[b] | 0.8 | | Ryd | | | | |
| IP[c] | 291.33($CH_2$) | | | | | | | |
| 6(sh)[d] | 292.2(3) | | 3.9 | | $\sigma^*$(C—F) | | | |
| 7 | 293.1 | | 3.0 | | 3*p* | 292.2 | | 3*s* |
| 8 | 294.7 | | 1.5 | | Ryd | | | |
| IP[c] | 296.10($CF_2$) | | | | | | | |
| 9 | 296.2 | −4.9 | | ?-1 | | | | |
| 10 | 299.3 | −8.0 | −3.2 | ?-2 | ?-1 | | | |
| 11 | 303(1) | −11.7 | −6.9 | $\sigma^*$(C=C) | ?-2 | | | |

$CHF=CF_2$

| | | | | | | Parent ion yield (Ref. 13) | | |
|---|---|---|---|---|---|---|---|---|
| | *E* | *T* (eV) | | Assignment | | *E* | Assignment | |
| No. | (±0.2 eV) | CHF | $CF_2$ | CHF | $CF_2$ | (±0.6 eV) | CHF | $CF_2$ |
| 1 | 287.6 | 6.2 | | $\pi^*$(C—C) | | 287.7 | $\pi^*$ | |
| 2 | 288.9[b] | 5.0 | | $\sigma^*$(C—F) | | | | |
| 3 | 289.7[a] | | 6.5 | | $\pi^*$(C—C) | 289.9 | | $\pi^*$ |
| 4(sh)[d] | 290.7 | 3.2 | | 3*p* | | | | |
| 5 | 291.6 | 2.3 | 4.7 | | $\sigma^*$(C—F) | 292.1 | 3*s* | |
| 6 | 292.4 | | 3.9 | 4*p* | 3*s* | | | |
| IP[c] | 293.87(CHF) | | | | | | | |
| 7 | 294.0 | | 2.3 | | 3*p* | | | |
| 8(sh)[d] | 295.1 | | 1.1 | | 4*p* | | | |
| IP[c] | 296.25($CF_2$) | | | | | | | |
| 9 | 296.3 | −2.3 | | ?-1 | | | | |
| 10 | 298.0 | −4.1 | −1.7 | ?-2 | ?-1 | | | |
| 11 | 300.8 | | −4.5 | | ?-2 | | | |
| 12(sh)[d] | 304(1) | −10 | | $\sigma^*$(C=C) | | | | |

[a]Calibration: The indicated feature is located 2.45 eV below (C 1*s*,$\pi^*$) of CO in $CH_2CHF$, 2.18 eV above (C 1*s*,$\pi^*$) of CO in $CH_2CF_2$, and 1.10 eV below (C 1*s*,$\pi^*$) of $CO_2$ in $CHFCF_2$.

[b]Existence and energy deduced from least-squares curve fitting.

[c]From XPS (Ref. 45).

[d]sh= shoulder.

is not planar (approximately 25° twist), and the C—C bond is stretched by 0.05 Å, the geometry change which produces the major vibrational excitation is a C—H contraction which probably arises from the increased effective nuclear charge and thus an overall valence-shell contraction rather than a specific antibonding property of the $\pi^*$ orbital.

Excitations from C 1$s$(CHF) and C 1$s$($CF_2$) to $\sigma^*$(C—F) in $CHFCH_2$, $CH_2CF_2$, and $CHFCF_2$ have been identified on the basis of term values, the bond-length correlation, and comparisons among the spectra. In some cases the $\sigma^*$(C—F) transitions are assigned to shoulders or peaks in apparently unstructured regions which have been revealed by curve fitting (Fig. 6). Our interpretation of the structure in the pre-edge region of the spectrum of $CHFCH_2$ is confirmed by the recent high-resolution ISEELS obtained by Sze *et al.*[53] In particular, the peak (No. 3) that we identify by curve fitting at 288.3 eV in the dip between the prominent features 2 and 4 is clearly resolved in their work. In addition they observe two highly structured bands corresponding to the broad regions of intensity we have identified as features 4 and 5.

The term values and oscillator strengths of the $\sigma^*$(C—F) features are listed in Table VII and the trends in these quantities are discussed in detail in Secs. V F and V H. We note here that the C $1s \rightarrow \sigma^*$(C—F) transition is always more intense when the core hole is on the more fluorinated carbon and that the (C $1s^{-1}$,$\sigma^*$(C—F)) term value increases somewhat with fluorination (from 3.8 eV in $CHFCH_2$ to 4.8 eV in $CF_2CF_2$) indicating that the $\sigma^*$(C—F) orbital is stabilized by the addition of fluorines. The trend of relatively constant $\pi^*$ and increasing $\sigma^*$(C—F) term value with fluorination is the same as that observed in the C 1$s$ spectra of the fluorobenzenes,[6] although the $\pi^*$ shift is larger and the $\sigma^*$ shift is smaller in the fluoroethenes than in the fluorobenzenes. This perfluoro effect is further evidence that the second excited level is primarily a $\sigma^*$(C—F) type of orbital. C $1s \rightarrow 3s$ and $3p$ Rydberg transitions in $CHFCH_2$, $CH_2CF_2$, and $CHFCF_2$ can be identified on the basis of term values although they overlap other features in these spectra. With our limited resolution the higher Rydberg transitions blend together to form a broad band of intensity leading up to the ionization threshold.

### C. Comparison to the C 1$s$ photoionization mass spectra of the fluoroethenes

The parent-ion ($M^+$) photoionization yield spectra of all the fluorinated ethenes reported by Beckmann *et al.*[13] exhibit C 1$s$ spectral features at very similar energies to those observed in the present work. For ease of comparison the positions of these features are listed in Tables II and III along with the assignments suggested by Beckmann *et al.* Although the $1s \rightarrow \pi^*$ energies in the ion yield spectra of *cis*-CHFCHF and $CH_2CF_2$ are 0.6 eV lower than our results, this difference is probably not significant since the energy scales of the photoion yield spectra are uncertain to ±0.6 eV because of difficulties in monochromator calibration.[54] The $M^+$ yield spectra might be expected to follow the photoabsorption curve below the 1$s$ IP, but dications and their fragments will be produced preferentially above the 1$s$ IP because of the Auger process. For most of the fluoroethenes the shapes of the $M^+$ yield and ISEELS-derived oscillator strengths are in general agreement. A discrepancy exists in the case of $CH_2CHF$ and $CH_2CF_2$ where there is an unexpected rise to the $M^+$ intensity at the C 1$s$($CH_2$) IP. More recent studies[54] suggest that this may be an artifact of the ion yield measurements associated with inadequate normalization of the structure in the photon flux spectrum caused by carbon contamination of the monochromator grating. In addition the relative intensities of the two $\pi^*$ transitions in the ion yield spectra of the intermediate fluoroethenes (particularly $CHFCF_2$) are different from those found in the ISEEL spectra. This suggests that site selective fragmentation may be occurring as has been documented in acetone[55] and $CH_3CF_3$.[56]

With regard to the assignments, the identification of the principal features as transitions from the various C 1$s$ levels to the $\pi^*$ orbital is the same in this work and that of Beckmann *et al.*[13] However, the features we describe as $\sigma^*$(C—F) have been attributed by these authors to 3$s$ or 3$d$ Rydberg transitions. In contrast, we identify the C $1s \rightarrow 3s$ transitions as weak shoulders to the relatively strong C $1s \rightarrow \sigma^*$(C—F) transitions. The existence of two separate features is clear in the expanded plots (Figs. 4 and 6), particularly in *cis*-CHFCHF and

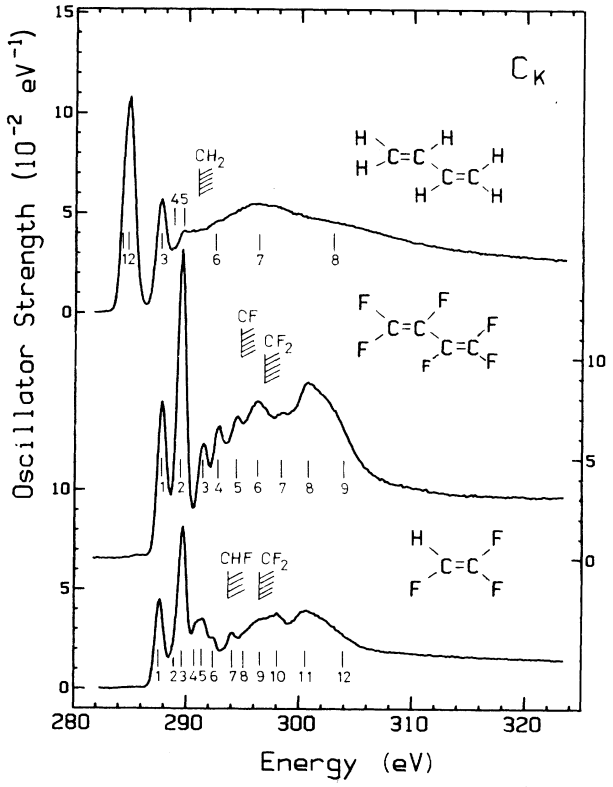


FIG. 7. Absolute oscillator strengths of 1,3-butadiene, 1,3-perfluorobutadiene, and trifluoroethene. See Fig. 3 caption for further details.

$C_2F_4$. The strong intensity of the features attributed to C $1s \rightarrow \sigma^*$(C—F) transitions as well as the bond-length correlation[4] make the valence labelling the more plausible assignment for the principle intensity in the $3s,\sigma^*$(C—F) region of the C $1s$ spectra of the fluoroethenes.

### D. C 1*s* spectrum of 1,3-perfluorobutadiene

The absolute oscillator strength spectrum of 1,3-perfluorobutadiene in the region of C $1s$ excitation is presented in Fig. 7 in comparison to the C $1s$ spectra of its unfluorinated analog, 1.3-*trans*-butadiene, and of $CHFCF_2$ which can be considered as one-half of 1,3-$C_4F_6$. Expansions and fits to the discrete regions of these spectra are presented in Fig. 8. The spectrum of 1,3-$C_4H_6$ has been reported previously at both low[11] and high[12] resolution. The C $1s(CH_2)$ and C $1s$(CH) IP's of 1,3-$C_4H_6$ have been estimated to be 290.4(3) eV.[11] The C $1s$ IP's of 1,3-$C_4F_6$ are not available in the literature to our knowledge. The C $1s(CF_2)$ IP has been estimated to be 296.6(4) eV, the average of the C $1s(CF_2)$ IP's in $CF_2CHF$, $CF_2CF_2$, and $CF_2CFCF_3$.[45] The C $1s$(CF) IP is estimated to be 294.4 eV, the average of the C $1s$(CF) IP's of $CF_2CFCF_3$ and $CHFCF_2$.[45] The observed energies, term values, and proposed assignments for the C $1s$ spectral features of the butadienes are listed in Table IV.

1,3-$C_4F_6$ has a nonplanar skew-*cis* ground-state geometry with a dihedral angle around 47°,[57,58] in contrast to the planar conformation of 1,3-*trans*-butadiene.[59] In this nonplanar conformation $\pi$ conjugation is reduced, and thus the C=C bond is shorter [1.336(18) as opposed to 1.344 Å in 1,3-$C_4H_6$] while the C—C bond is longer [1.488(18) as opposed to 1.467 Å].[57] If there is no $\pi$ conjugation, the C $1s$ spectrum of 1,3-$C_4F_6$ should be similar to that of $CHFCF_2$. The C $1s$ spectrum of 1,3-$C_4F_6$ is dominated by the first two peaks at low energy which are clearly C $1s$(CF)$\rightarrow\pi^*$(C=C) and C

TABLE IV. Absolute energies, term values, and proposed assignments for the C $1s$ spectral features of 1,3-*trans*butadiene and 1,3-perfluorobutadiene.

| | | | $CH_2=CHCH=CH_2$ | | |
|---|---|---|---|---|---|
| | | | Proposed assignment | | |
| | *E* | | *A*[a] | | *B*[b] |
| No. | (±0.2 eV) | *T* (eV) | 1*s*(CH) | 1*s*($CH_2$) | [1*s*(CH),1*s*($CH_2$)] |
| 1(sh) | 284.3[c] | 6.1 | $\pi^*a_u$ | | $\pi^*a_u$ |
| 2 | 284.8 | 5.6 | | $\pi^*a_u$ | $\pi^*b_g$ |
| 3 | 287.6 | 2.8 | $\pi^*b_g$ | $\pi^*b_g$ | 3*p* |
| 4 | 288.8 | 1.6 | 4*p* | 4*p* | 4*p* |
| 5 | 289.6 | 0.8 | Ryd | Ryd | Ryd |
| IP[d] | 290.4 | | | | |
| 6 | 292.4 | −2.0 | double excitation | double excitation | double excitation |
| 7 | 296.0 | −5.6 | $\sigma^*$(C—C) | $\sigma^*$(C—C) | $\sigma^*$(C—C) |
| 8 | 304 | −13 | $\sigma^*$(C=C) | $\sigma^*$(C=C) | $\sigma^*$(C=C) |

| | | | | $CF_2=CFCF=CF_2$ | | | |
|---|---|---|---|---|---|---|---|
| | | | | Proposed assignment | | | |
| | *E* | *T* (eV) | | *A* (preferred) | | *B* (alternate) | |
| No. | (±0.2 eV) | CF | $CF_2$ | CF | $CF_2$ | CF | $CF_2$ |
| 1 | 287.8 | 6.6 | | $\pi^*a''$ | | $\pi^*$ | |
| 2′ | 289.0 | | 5.4 | $\pi^*a'$ | | | |
| 2 | 289.5[c] | 4.6 | 6.9 | | $\pi^*a''$ | | $\pi^*(a'',a')$ |
| 3 | 291.5 | 2.9 | 4.9 | $\sigma^*$(C—F) | $\pi^*a'$ | $\sigma^*$(C—F) | |
| 4 | 292.7 | 1.7 | 3.9 | 3*p* | $\sigma^*$(C—F) | 3*p* | $\sigma^*$(C—F) |
| 5 | 294.4 | | 2.0 | | 3*p* | | 3*p* |
| IP[d] | 294.4(CF) | | | | | | |
| 6 | 296.3 | −1.9 | | ?-1 | | | |
| IP[d] | 296.6($CF_2$) | | | | | | |
| 7 | 298.5 | −4.1 | −1.9 | $\sigma^*$(C—C) | ?-1 | | |
| 8 | 300.7 | −6.3 | −4.1 | ?-2 | $\sigma^*$(C—C) | | |
| 9(sh) | 304(1) | −10 | −7 | $\sigma^*$(C=C) | $\sigma^*$(C=C),?-2 | | |

[a]Proposed by Lindholm (Ref. 60) and adopted in this work.
[b]Original assignments of Hitchcock *et al.* (Ref. 11) and Sodhi and Brion (Ref. 12).
[c]From high-resolution ISEELS (Ref. 12). The fit to the present data (Fig. 8) gave an energy of 284.1 eV but the intensity is too low.
[d]Estimated from XPS IP's of similar compounds (Ref. 45), see text.
[e]This feature is located 2.12(4) eV above (C $1s^{-1},\pi^*$) of CO [287.40(2)] (Ref. 22).

$1s(CF_2) \rightarrow \pi^*(C{=}C)$ transitions. There are two $\pi^*(C{=}C)$ levels, of $a''$ and $a'$ symmetry which correlate with the $a_u$ and $b_g$ $\pi^*$ orbitals of planar *trans*-butadiene. The nonplanar geometry of 1,3-$C_4F_6$ suggests that the splitting of these $\pi^*$ levels might be rather small and thus one possible assignment is to attribute transitions to both $\pi^*$ levels as overlapping in the same peak. For this to be correct, the two $\pi^*$ orbitals must be very nearly coincident in energy in order to explain the narrowness and symmetry of the $\pi^*$ peaks in the C $1s$ spectrum (features separated by less than 0.3 eV would not give rise to detectable changes in our spectrum because of the instrumental resolution of 0.6 eV). The similarity of the relative intensities of the first two $\pi^*$ features of 1,3-$C_4F_6$ to the $\pi^*$ transitions in $CHF{=}CF_2$ supports the conjecture of overlapping $1s \rightarrow \pi^*(a'',a')$ transitions in 1,3-$C_4F_6$. However, we prefer a different assignment for the reasons outlined below.

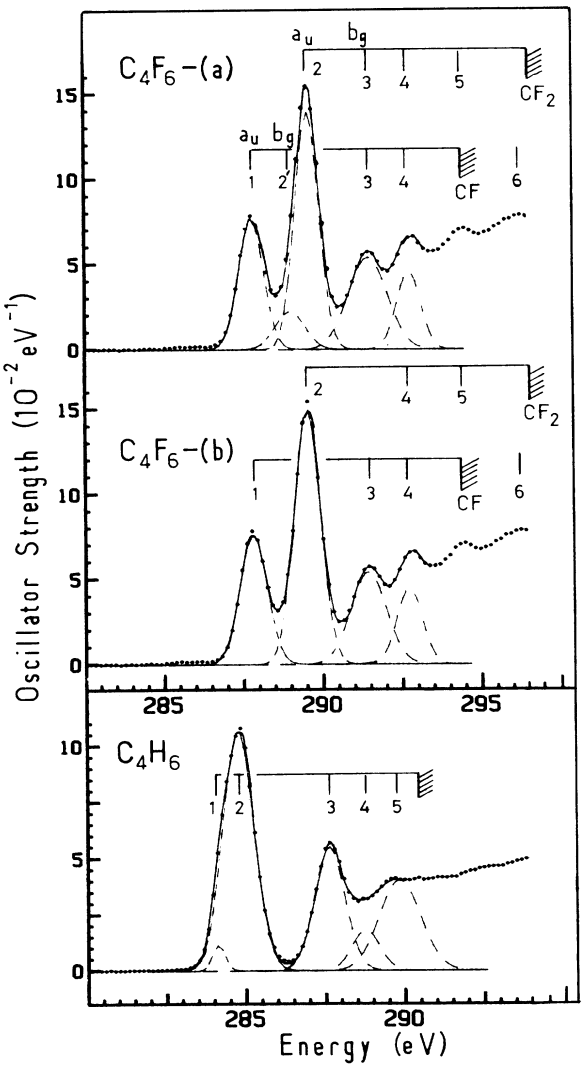


FIG. 8. Expansions of the spectra presented in Fig. 7. Points and dashed and solid lines as in Fig. 4. 1,3-$C_4F_6$ (a) corresponds to the preferred $\pi^*$ assignment and the fit has a $\chi^2$ of 0.45. 1,3-$C_4F_6$ (b) corresponds to the alternate $\pi^*$ assignment and the fit has a $\chi^2$ of 1.25.

In the high-resolution C $1s$ ISEEL spectrum of 1,3-butadiene,[12] the first peak shows a low-energy shoulder separated by 0.51(8) eV. Sodhi and Brion have interpreted this within a frozen orbital approximation as the separation of the two $\pi^*$ orbitals in 1,3-$C_4H_6$. However, Lindholm[60] has recently proposed an alternate interpretation of this spectrum. Based on hydrogenic-atoms-in-molecules (HAM/3) calculations and comparison with electron transmission resonances,[61] he suggests that the first shoulder reflects the separation of the (C $1s(CH)^{-1},\pi^*a_u$) and (C $1s(CH_2)^{-1},\pi^*a_u$) states while the two C $1s \rightarrow \pi^*b_g$ transitions overlap to form the higher-energy band (No. 3 in Figs. 7 and 8) resulting in a $\pi^*a_u$-$\pi^*b_g$ splitting of approximately 3.1 eV. By analogy with this interpretation one could alternately assign the first band in the C $1s$ spectrum of 1,3-$C_4F_6$ to C $1s(CF) \rightarrow \pi^*a''$ transitions, the second as the overlap of (C $1s(CF)^{-1},\pi^*a'$) and (C $1s(CF_2)^{-1},\pi^*a''$), and the third as (C $1s(CF_2)^{-1},\pi^*a'$). In fact the spectrum is fitted significantly better with four rather than three peaks between 285 and 292 eV [compare Fig. 8(a) and 8(b)]—i.e., with the addition of a low-energy shoulder on the second band. These four peaks are proposed in Table IV as the preferred assignment of the $1s \rightarrow \pi^*$ transitions in 1,3-$C_4F_6$. This implies a $\pi^*a''$-$\pi^*a'$ splitting of approximately 1.8 eV which is smaller than Lindholm assigns for 1,3-*trans*-butadiene and thus reasonable for the decreased conjugation in a nonplanar $\pi$ system. Although the electron transmission spectrum of 1,3-$C_4F_6$ has not been reported, its dissociative electron attachment spectra[62] exhibit resonances at 0 eV in the $C_4F_6^-$ channel and around 1.5 eV in the $C_3F_3^-$ and $F^-$ channels. If these features are $\pi^*$ resonances, they indicate a $\pi^*a''$-$\pi^*a'$ splitting of 1.5 eV, similar to the separation of the $a''$ and $a'$ (C $1s^{-1},\pi^*$) states according to our preferred assignment. Recent *ab initio* calculations[63] indicate that the $a''$ and $a'$ $\pi^*$ orbitals of 1,3-$C_4F_6$ are separated by 1.8 eV, further supporting our assignment. In addition, the occupied $\pi$ orbitals of 1,3-$C_4F_6$ are separated by 1.0 eV, roughly one third of the corresponding $\pi$ separation in 1,3-$C_4H_6$.[58]

With regard to intensities, according to HAM/3 calculations,[60] the $\pi^*a_u$ orbital of 1,3-$C_4H_6$ is delocalized on both carbon sites [C $2p$ linear combination of atomic orbitals (LCAO) coefficients of 0.42 (CH) and 0.51 ($CH_2$)] while the $\pi^*b_g$ is concentrated at the center (CH) carbon [C $2p$ LCAO coefficients of 0.43 (CH) and 0.25 ($CH_2$)]. Although the $\pi^*$ orbitals of 1,3-$C_4F_6$ will have a somewhat different spatial distribution, these results for 1,3-$C_4H_6$ can be used for a crude first approximation to the expected relative intensities for the C $1s \rightarrow \pi^*$ transitions in 1,3-$C_4F_6$. The squared $2p$ coefficients predict relative intensities of the order of 1:2.5:0.3 which are in reasonable agreement with the observed relative intensities [1:2:$<$1] since the third peak overlaps the C $1s(CF) \rightarrow \sigma^*(C{-}F)$ transition. The oscillator strengths of the $\pi^*$ features in 1,3-perfluorobutadiene (based on both assignments) are listed in Table VI. The values based on the alternate assignment are in somewhat

better agreement with the trends from the fluoroethenes, although the OS based on our preferred assignment are not grossly different.

The term values of the C $1s \rightarrow \pi^*(C{=}C)$ transitions of 1,3-$C_4F_6$ (average values of 6.7 and 5.2 eV) are similar to those of the fluoroethenes (5.9–6.5 eV) consistent with a minimal influence of fluorine substitution on the $\pi^*$ orbitals. These 1,3-$C_4F_6$ $\pi^*$ values are somewhat higher than those in 1,3-$C_4H_6$ $\pi^*$ (5.8 and 2.8 eV). This is consistent with a smaller $\pi$-$\pi^*$ splitting because of the nonplanar geometry.

The C $1s \rightarrow \sigma^*(C{-}F)$ transitions are attributed to bands 3 and 4 which have term values similar to those in the fluoroethenes. The C $1s(CF) \rightarrow \sigma^*(C{=}C)$ transition is assigned to the broad high-energy shoulder (No. 9) analogous to our assignments in 1,3-$C_4H_6$ and the fluoroethenes. Dixon[63] calculates three $\sigma^*$ levels between the two $\pi^*$ orbitals in 1,3-$C_4F_6$ but we see no signs of transitions to these in our spectra. According to the bond-length correlation,[4] the C $1s \rightarrow \sigma^*(C{-}C)$ transitions are expected about 4 eV above each C 1*s* IP, as observed in 1,3-$C_4H_6$. However, these seem to be submerged under other strong features which correspond to the ?-1 and ?-2 bands in the fluoroethenes.

### E. F 1*s* spectra of the fluoroethenes and 1,3-perfluorobutadiene

The absolute oscillator strengths of all five fluoroethenes and 1,3-$C_4F_6$ in the region of F 1*s* excitation are presented in Fig. 9 on an absolute energy scale. The F 1*s* IP's of $CHFCH_2$, $CH_2CF_2$, $CHFCF_2$, and $C_2F_4$ have been determined by XPS.[45] The F 1*s* IP of *cis*-CHFCHF is estimated from those of $CHFCH_2$ and $CHFCF_2$ while the F 1*s* IP's of 1,3-$C_4F_6$ are taken to be the same as those of $CHFCF_2$. The energies, term values, and proposed assignments of all the F 1*s* spectral features are listed in Table V.

TABLE V. Absolute energies, term values, and proposed assignments for the F 1*s* spectral features. (a) *cis*CHFCHF, and $CF_2CF_2$, (b) $CHFCH_2$ and $CH_2CF_2$ and (c) $CHFCF_2$ and 1,3-$C_4F_6$.

(a)

| No. | *cis*CHF=CHF *E* | *T* | No. | $CF_2{=}CF_2$ *E* | *T* | Proposed assignment |
|---|---|---|---|---|---|---|
| 1 | 689.3[a] | 4.4 | 1 | 690.7[a] | 4.3 | $\pi^*(C{=}C)$ |
| 2 | 691.4 | 2.3 | 2 | 692.2 | 2.8 | $\sigma^*(C{-}F)$ |
| | | | 3(sh) | 693.7 | 1.3 | 4*p* |
| IP | 693.7[b] | | IP | 695.0[c] | | |
| 3 | 697(1) | −3.3 | 4 | 696.1(4) | −1.1 | ?-1 |
| 4 | 701(2) | −7 | 5 | 702.6(4) | −7.5 | ?-2 |
| 5 | 702(2) | −26 | 6 | 718(1) | −23 | EXAFS(C—F) |

(b)

| No. | $CHFCH_2$ (±2.0 eV) | *T* | No. | $CH_2CF_2$ (±0.2 eV) | *T* | Proposed assignment |
|---|---|---|---|---|---|---|
| 1 | 689.2 | 4.1 | 1 | 690.3 | 4.2 | $\pi^*(C{=}C)$ |
| 2 | 690.6[a] | 2.7 | 2 | 692.3[a] | 2.2 | $\sigma^*(C{-}F)$ |
| IP | 693.26[c] | | IP | 694.44[c] | | |
| 3 | 696(2) | −3 | 3(sh) | 696.4(2) | −2.0 | ?-1 |
| | | | 4 | 703(1) | −8.6 | ?-2 |
| 4 | 716(2) | −23 | 5 | 719(2) | −25 | EXAFS(C—F) |

(c)

| | $CHFCF_2$ | | | 1,3-$C_4F_6$ | | | Proposed assignment | |
|---|---|---|---|---|---|---|---|---|
| | *E* | *T* (eV) | | *E* | *T* (eV) | | | |
| No. | (±0.2 eV) | CHF | $CF_2$ | (±0.2 eV) | CHF | $CF_2$ | CHF | $CF_2$ |
| 1 | 690.3[a] | 3.8 | 4.5 | 689.9[a] | 4.2 | 4.9 | $\pi^*(C{-}C)$ | $\pi^*(C{=}C)$ |
| 2 | 692.2 | 1.9 | 2.6 | 692.6 | 1.5 | 2.2 | $\sigma^*(C{-}F)$ | $\sigma^*(C{-}F)$ |
| IP(CHF) | 694.1[c] | | | 694.1[d] | | | | |
| 3(sh) | 694.4 | −0.3 | 0.4 | 696(1) | −1.5 | −1.5 | ?-1 | ?-1 |
| IP($CF_2$) | 694.8[c] | | | 694.8[d] | | | | |
| 4 | 702(1) | −7.5 | −7.5 | 701.4(9) | −6.9 | −6.9 | ?-2 | ?-2 |
| 5 | 716(1) | −22 | −22 | 718(1) | −23 | −23 | EXAFS (C-F) | EXAFS (C—F) |

[a]Calibration in terms of energy of the indicated feature relative to the (O $1s^{-1}, \pi^*$) state of CO [534.2 eV (Ref. 22)]: CHFCHF [155.1(2) eV], $CF_2CF_2$ [156.5(2) eV], $CHFCH_2$ [156.4(2) eV], $CH_2CF_2$ [158.1(1) eV], $CHFCF_2$ [156.1(2) eV], 1,3-$C_4F_6$ [155.7(1) eV].
[b]Estimated as the average of the F 1*s*(CHF) IP's of $CHFCH_2$ (693.26 eV) and $CHFCF_2$ (694.1 eV) (Ref. 45).
[c]From XPS (Ref. 45).
[d]IP's estimated to be the same as those of $CHFCF_2$ (Ref. 45).

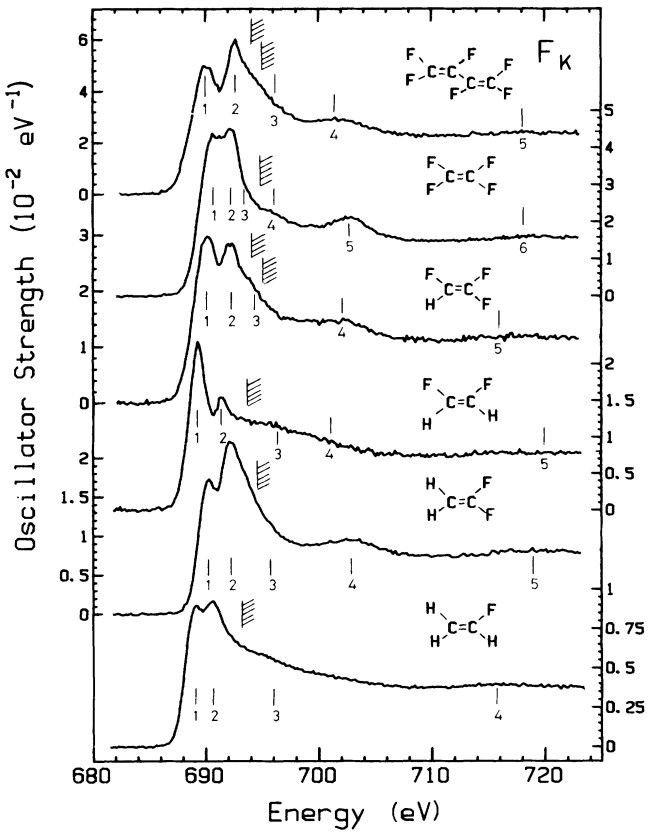


FIG. 9. Absolute oscillator strengths of $CHFCH_2$, *cis*-CHFCHF, $CF_2CF_2$, $CHFCF_2$, $C_2F_4$, and 1,3-$C_2F_6$ in the region of F 1*s* excitation. See Fig. 3 caption for further details.

The lowest-energy feature in each F 1*s* spectrum is assigned to F $1s \rightarrow \pi^*(C{=}C)$ transitions. These features are broader (FWHM $\sim$2 eV) than the corresponding C $1s \rightarrow \pi^*$ transitions (FWHM $\sim$1 eV). The increase in width is much greater than expected from the shorter F 1*s* core hole lifetime. This suggests either that the (F $1s^{-1}, \pi^*$) state has a geometry very different from that of the ground state, possibly with a steep dissociative upper-state potential curve, or that transitions to another state [possibly (F $1s^{-1}, 3s$] contribute appreciably at a similar energy. The (F $1s^{-1}, \pi^*$) term values are systematically 2 eV lower than the (C $1s^{-1}, \pi^*$) term values.

The second peak in each spectrum, which is assigned to F $1s \rightarrow \sigma^*(C{-}F)$ transitions, is generally more intense than feature 1 ($\pi^*$). This is consistent with our expectation that the F 1*s* orbital will have better spatial overlap with a $\sigma^*(C{-}F)$ than with a $\pi^*(C{=}C)$ orbital. Both $CHFCF_2$ and 1,3-$C_4F_6$ have two fluorine environments with F 1*s* IP's separated by 0.7 eV and thus the $\sigma^*(C{-}F)$ and $\pi^*$ features should be additionally broadened in these species. We cannot explain the anomalously small intensity of the F $1s \rightarrow \sigma^*(C{-}F)$ transition (feature 2) in *cis*-CHFCHF. This spectrum was recorded six times on two separate occasions, always with the same result. As with the F $1s \rightarrow \pi^*$ transitions, the F $1s \rightarrow \sigma^*(C{-}F)$ term values are consistently 1–2 eV smaller than the corresponding C $1s \rightarrow \sigma^*(C{-}F)$ ones, indicating a characteristic influence of the core hole relaxation on the state energies. The trends in F $1s \rightarrow \pi^*$ and F $1s \rightarrow \sigma^*(C{-}F)$ intensities are discussed further in Secs. V G and V H.

F $1s \rightarrow \sigma^*(C{=}C)$ excitations would be expected to be observed 10–12 eV above the F 1*s* IP if there was significant delocalization of the $\sigma^*(C{=}C)$ MO onto the fluorines (i.e., mixing of $\sigma^*(C{-}F)$ and $\sigma^*(C{=}C)$, one of the possible explanations for the ?-1 and ?-2 features in the C 1*s* spectra). Feature 5 of $C_2F_4$ and feature 4 in all the other fluoroethenes except $CH_2CHF$, at 7–9 eV above the IP, are possibilities for transitions of this type. However, these features seem to be too low in energy to be F $1s \rightarrow \sigma^*(C{=}C)$. In addition, the low intensity of feature 4 in *cis*-CHFCHF and the absence of this peak in $CH_2CHF$ argue against this assignment. From their term values these rather prominent features appear to correspond to the F $1s \rightarrow$?-2 transitions. Thus they could arise from transitions to a second $\sigma^*(C{-}F)$ level, one of the suggestions we have made for the C $1s \rightarrow$?-2 feature. The absence of this feature in $CH_2CHF$ and its weak intensity in *cis*-CHFCHF are consistent with this interpretation. An alternate possibility is that this feature is the first EXAFS oscillation associated with backscattering from adjacent fluorines. Again the absence in $CH_2CHF$ is consistent with this. In all five fluoroethenes there is a shoulder (No. 3) on the high-energy side of the F $1s \rightarrow \sigma^*(C{-}F)$ transition, which we attribute to the F $1s \rightarrow$?-1 transition. High in the continuum, about 23 eV above the IP, there is a broad maximum in each spectrum. This is likely a conventional EXAFS feature associated with backscattering from adjacent atoms.

The F 1*s* spectrum of 1,3-$C_4F_6$ contains two features below the IP which are attributed to the F $1s \rightarrow \pi^*$ and F $1s \rightarrow \sigma^*$ transitions, respectively. The first feature is broader, at somewhat lower energy and higher term value than the features attributed to F $1s \rightarrow \pi^*(C{=}C)$ transitions in the fluoroethenes. This may reflect the 1.8-eV splitting of the $a''$ and $a'$ $\pi^*$ levels deduced from the C 1*s* spectrum. As with the fluoroethenes, the F $1s \rightarrow \pi^*$ term value of 1,3-$C_4F_6$ is consistently lower than the C $1s \rightarrow \pi^*$ term value. The F 1*s* continuum of 1,3-$C_4F_6$ exhibits a prominent, broad feature about 7 eV above the estimated F 1*s* IP. This feature is well aligned with that attributed to F $1s \rightarrow$?-2 in the spectra of all fluoroethenes which contain two or more fluorine atoms.

### F. Trends in C $1s \rightarrow \pi^*(C{=}C)$ and C $1s \rightarrow \sigma^*(C{-}F)$ term values

The term values of the C $1s \rightarrow \pi^*$ and C $1s \rightarrow \sigma^*(C{-}F)$ transitions are summarized in Tables VI and VII and plotted in Fig. 10 to illustrate the trends with location of the core hole and the degree of fluorine substitution. Within a frozen orbital approximation (Koopman's theorem) the negative term value represents the $\pi^*$ and $\sigma^*$ orbital energies. The rapid decline of the $\sigma^*(C{-}F)$

TABLE VI. $1s \rightarrow \pi^*$ term values and oscillator strengths.

| Species | | Term values (eV) $CH_2$ C | CHF C | CHF F | $CF_2$ C | $CF_2$ F | ETS[c] | Oscillator strengths ($10^{-2}$)[a,b] $CH_2$ C | CHF C | CHF F | $CF_2$ C | $CF_2$ F | $\Sigma f$ C 1s | $\Sigma f$ F 1s |
|---|---|---|---|---|---|---|---|---|---|---|---|---|---|---|
| $CH_2CH_2$ | | 6.3 | | | | | −1.8 | 3.4 | | | | | 6.8 | 0 |
| $CH_2CHF$ | | 6.1 | 6.4 | 4.1 | | | −1.9 | 3.4 | 5.1 | 0.7 | | | 8.5 | 0.7 |
| CHFCHF | | | 6.4 | 4.4 | | | | | 4.6 | 2.3 | | | 9.2 | 4.6 |
| $CH_2CF_2$ | | 5.9 | | | 6.5 | 4.2 | −2.4 | 3.4 | | | 6.9 | 0.9 | 10.2 | 1.9 |
| $CHFCF_2$ | | | 6.3 | 3.8 | 6.5 | 4.5 | −2.5 | | 4.0 | 2.5[d] | 6.6 | 2.4[e] | 10.6 | 7.4 |
| $CF_2CF_2$ | | | | | 6.4 | 4.3 | −3.0 | | | | 5.7 | 2.5 | 11.3 | 10 |
| $C_4H_6$ | $A$[e]-$a_u$ | 5.8 | | | | | −0.6 | 3.4 | | | | | 20.3 | |
| | $A$[e]-$b_g$ | 2.8 | | | | | −2.8 | 1.6 | | | | | | |
| | $B$[f] | 5.8 | | | | | | 3.4 | | | | | 14 | |
| $C_4F_6$ | $A$[e]-$a''$ | | 6.6 | 4.6 | 6.9 | 4.4 | | | 3.8 | 2.5[d] | 6.6 | 2.5[d] | 28 | 15 |
| | $A$[e]-$a'$ | | 4.9 | | 4.9 | | | | 1.3 | | 2.1[g] | | | |
| | $B$[f] | | 6.9 | 4.6 | 6.9 | 4.4 | | | 4.1 | 2.5[d] | 7.7 | 2.5[d] | 24 | 15 |

[a]From the area of Gaussian peaks least-squares fitted to the oscillator strength spectra.
[b]Except for the final two columns, the measured oscillator strengths have been divided by the number of core-excited atoms contributing to the feature and thus the intensities are on a per-transition basis. The last two columns give the total C $1s \rightarrow \pi^*$ and F $1s \rightarrow \pi^*$ intensity, respectively.
[c]Negative ion resonances from electron transmission spectroscopy (ETS) Refs. 52 and 64.
[d]No attempt has been made to partition the F 1s(CHF) and F 1s($CF_2$) intensities.
[e]Based on the preferred assignment of the $\pi^*$ transitions ($A$ of Table IV).
[f]Based on the alternate assignment of the $\pi^*$ transitions ($B$ of Table IV).
[g]We have assumed that 50% of peak 4 in 1,3-$C_4F_6$ is from the C 1s($CF_2$)$\rightarrow\pi^*(a')$ transition.

energy and the relative constancy of the $\pi^*$ energy with increased fluorination clearly supports the extension of the concepts of the perfluoro effect from occupied to unoccupied orbitals as has been proposed recently.[6,14] The remarkable constancy of the (C $1s^{-1},\pi^*$) term values in all three molecules indicates that the addition of a relatively strong C—F dipole has negligible influence on the energy of a $\pi^*$ orbital which is orthogonal to the added dipole. This contrasts with nonplanar perfluoro-unsaturates, such as $CF_3C{\equiv}CCF_3$, $CF_3CO_2H$, and $CF_3CF{=}CFCF_3$, where the $\pi^*$ term values are several eV lower than in their hydrocarbon counterparts.[14] The constancy of the $\pi^*$ term values in the fluoroethenes is reminiscent of the fluorobenzenes[6] although the two cases are not completely parallel since the C 1s(CH) and C 1s(CF) term values (i.e., approximate $\pi^*$ orbital energies) increase in the fluorobenzenes by 0.2 eV per added fluorine whereas in the fluoroethenes the C 1s($CH_2$), C 1s(CHF), and C 1s($CF_2$)$\rightarrow\pi^*$ term values decrease by 0.2, 0.05, and 0.05 eV per added fluorine, respectively.

The effects of fluorination on the $\pi^*$ term values are most evident in the spectrum of $CH_2CF_2$ (Figs. 5 and 6, Table III) where there is a difference of 0.6 eV between the term values of the C 1s($CH_2$)$\rightarrow\pi^*$ ($T$=5.9 eV) and the C 1s($CF_2$)$\rightarrow\pi^*$ ($T$=6.5 eV) transitions. The C $1s \rightarrow \pi^*$ intensities (Sec. V G) indicate that the $\pi^*$ orbital has greater electron density on the $CF_2$ than on the $CH_2$ carbon. This difference in electron density may lead to different relaxation energies for the (C 1s($CH_2$)$^{-1},\pi^*$)

TABLE VII. $1s \rightarrow \sigma^*$(C—F) term values and oscillator strengths.

| Species | Term values (eV) CHF C | CHF F | $CF_2$ C | $CF_2$ F | C 1s oscillator strengths ($10^{-2}$)[a] CHF C | $CF_2$ C | $\Sigma f$ |
|---|---|---|---|---|---|---|---|
| $CH_2CHF$ | 3.8 | 2.7 | | | (2.7)[b] | | (2.7)[b] |
| $CH_2CF_2$ | | | 3.9 | 2.2 | | (4)[b] | (4)[b] |
| CHFCHF | 4.6 | 2.3 | | | 2.8[c] | | 5.6 |
| $CHFCF_2$ | 5.0 | 1.9 | 4.7 | 2.6 | 2.1 | 4.2 | 6.3 |
| $CF_2CF_2$ | | | 4.8 | 2.6 | | 4.7[c] | 9.4 |
| 1,3-$C_4F_6$ | 2.9 | 1.8 | 3.9 | 2.2[b] | (2.1)[d] | 2.2 | 6.6 |

[a]From the area of Gaussian peaks least-squares fitted to the oscillator strength spectra.
[b]Value uncertain due to peak overlap.
[c]These values are divided by 2 to give the oscillator strength per carbon.
[d]This assumes that 50% of peak 4 in 1,3-$C_4F_6$ is from the C 1s(CF)$\rightarrow\sigma^*$(C—F) transition.

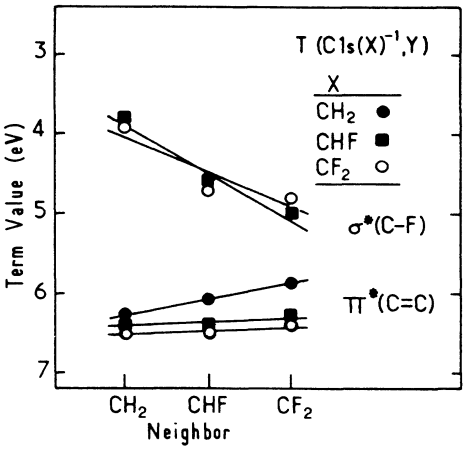


FIG. 10. The term values of the C $1s \rightarrow \sigma^*$(C—F) and C $1s \rightarrow \pi^*$ transitions plotted as a function of the core hole ($X$) and the degree of fluorination of the neighboring carbon.

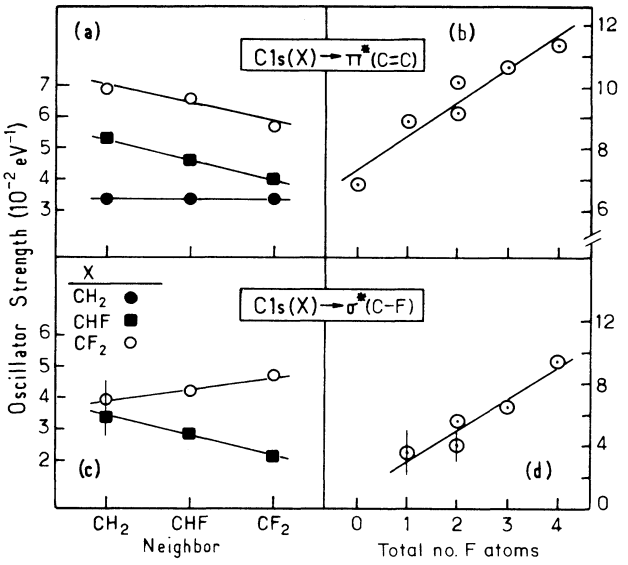


FIG. 11. Trends in the $\pi^*$(C=C) and $\sigma^*$(C—F) oscillator strengths. (a) C $1s \rightarrow \pi^*$ intensity as a function of the core hole ($X$) and the degree of fluorination of the neighboring carbon, (b) total C $1s \rightarrow \pi^*$ intensity as a function of the number of fluorines, (c) C $1s \rightarrow \sigma^*$(C—F) intensity as a function of the core hole ($X$) and the degree of fluorination of the neighboring carbon, (d) total C $1s \rightarrow \sigma^*$(C—F) intensity as a function of the number of fluorines.

and (C $1s(CF_2)^{-1}, \pi^*$) states which may be the origin of this shift. The relatively constant term value for the C $1s \rightarrow \pi^*$ transition throughout this series contrasts sharply with the systematic increase from 1.8 to 3.0 eV observed in the position of the $\pi^*$ negative ion resonance in electron transmission spectra of the fluoroethenes.[52,64] This suggests that the usual assumption of a constant shift between core excitation and negative ion resonances involving the same virtual level is not completely valid in this instance. The difference may be related to different geometries for the core excited and negative ion species.

### G. Oscillator strengths of the $1s \rightarrow \pi^*$ transitions

The oscillator strengths of the C $1s \rightarrow \pi^*$ transitions (summarized in Table VI) can be considered as a probe of the spatial distribution of the $\pi^*$ orbital. This may change from molecule to molecule either because of unequal sharing between different carbon sites in the case of the lower symmetry species or because of compression of the $\pi^*$ orbital towards the molecular core, if the potential barrier increases with fluorination. Absolute C $1s \rightarrow \pi^*$ OS were obtained from the areas of the fitted Gaussian line shapes (see Figs. 4, 6, and 8). This allowed more precise intensity determination in cases of overlapping features. In Fig. 11(a) and 11(b) the C $1s(X) \rightarrow \pi^*$ oscillator strengths are plotted both on a per-site basis, as a function of the type of neighbor, and as the variation of the total C $1s \rightarrow \pi^*$OS with fluorination.

There is a systematic increase in the *total* C $1s \rightarrow \pi^*$ OS [i.e., the sum of the C $1s$(CHF)$\rightarrow \pi^*$ and C $1s(CF_2) \rightarrow \pi^*$ OS in $CH_2CF_2$] with addition of fluorines such that the oscillator strength for the C $1s \rightarrow \pi^*$ transition of $C_2F_4$ is 65% greater than that for $C_2H_4$. This increase with fluorination is consistent with the development of a stronger potential barrier in the more highly fluorinated species. Although the fluorine atoms in the fluoroethenes do not provide a complete cage for the carbon atoms, even in $C_2F_4$, the systematic increase throughout the series of the C $1s \rightarrow \pi^*$ intensities [and also the C $1s \rightarrow \sigma^*$(C—F) transitions (see Sec. V H)] is clear evidence of potential barrier effects. The trend with fluorination in the total C $1s \rightarrow \pi^*$ intensity is analogous to the enhancement of C $1s \rightarrow \sigma^*$(C—F) transitions with increased enclosure of a carbon by fluorines, which has been demonstrated recently through a comparison of the ISEELS-derived oscillator strengths of $C_6F_6$, $C_2F_4$, $C_2F_6$, and $CF_4$.[65] Localization of the $\pi^*$ orbital on the more highly fluorinated carbon is also found in the fluorobenzenes where the mean ratio of C $1s$(CF)$\rightarrow \pi^*$ to C $1s$(CH)$\rightarrow \pi^*$ intensities is 1.3.[6]

We note that the trend of increasing intensity with fluorination occurs only in the *total* C $1s \rightarrow \pi^*$ oscillator strength [Fig. 11(b)] or when comparing different C $1s(X)$ types. In contrast, the intensities of transitions to $\pi^*$ from a single carbon type show the *opposite* trend in that, for excitations from both C $1s$(CHF) and C $1s(CF_2)$ to $\pi^*$, the intensity decreases as the neighboring carbon is increasingly fluorinated [see Fig. 11(a)]. This effect can be explained either in terms of a shift of the $\pi^*$ spatial distribution towards the more fluorinated carbon because the fluorination of a neighboring carbon polarizes the $\pi^*$ orbital, or alternatively because the stronger potential barrier on the more fluorinated carbons effectively compresses the $\pi^*$ orbital to give better overlap with the core. The fact that the C $1s(CH_2) \rightarrow \pi^*$ intensity is independent of the degree of fluorination of its neighbor suggests that the electron density is not rearranged appreciably so that the latter explanation seems

more reasonable. A third possibility is that the $\pi^*$ orbital has a similar spatial distribution in all of the molecules and it is the C 1*s* orbital which expands with fluorination. However, fluorination will contract rather than expand the C 1*s* orbital and in general one expects valence orbitals to be much more sensitive than core orbitals to changes in the molecular structure.

The intensities of the C $1s \rightarrow \pi^*$ transitions in 1,3-$C_4F_6$ are summarized in Table VI and have been discussed in Sec. V D with regard to the two possible assignments. Both the intensity per transition and the total intensity are consistent with the trends observed in the fluoroethenes, particularly within the alternate assignment which assumes that the *a''-a'* splitting is small and thus all of the C $1s \rightarrow \pi^*$ intensity is contained in the first two features.

The features assigned to F $1s \rightarrow \pi^*$ transitions are remarkably intense, having an oscillator strength typically 50% as large as that of the C $1s \rightarrow \pi^*$ transition. We believe this does not reflect the spatial distribution of the $\pi^*$ orbital in the ground state but rather is an effect of relaxation which distorts the $\pi^*$ density distribution towards a F 1*s* hole. An apparently similar, anomalously large F $1s \rightarrow \pi^*$(CO) intensity was observed recently in a study of the $1s \rightarrow \pi^*$(CO) intensities in HCO*X*, $X = NH_2$, OH, and F.[19]

### H. Oscillator strengths of the $1s \rightarrow \sigma^*$ transitions

The C $1s \rightarrow \sigma^*$(C—F) oscillator strengths are summarized in Table VII and plotted in Fig. 11(c) and 11(d). Although these values are less precise than those for the C $1s \rightarrow \pi^*$ transitions because of peak overlap, they do exhibit systematic trends. We have not attempted to derive F $1s \rightarrow \sigma^*$(C—F) OS since their overlap with other features is too great for reliable fitting. The total C $1s \rightarrow \sigma^*$(C—F) intensity increases throughout the series, as was observed for the C $1s \rightarrow \pi^*$ transitions. This increase is consistent with the potential barrier effect and increased localization of the $\sigma^*$(C—F) orbital on the molecular core with increased fluorination. The greater intensity of C $1s(CF_2)$ than C 1*s*(CF)$\rightarrow\sigma^*$(C—F) transitions can also be attributed to the influence of the potential barrier. The trends with the type of neighbor in the intensities of the C 1*s*(CF)$\rightarrow\sigma^*$(C—F) and C $1s(CF_2)\rightarrow\sigma^*$(C—F) transitions are opposite one another. This may reflect only the limited precision of the intensity determination due to peak overlap. In general a reduced influence of the type of neighbor would be expected since the $\sigma^*$(C—F) orbital is further away than the $\pi^*$ orbital from the adjacent carbon.

With regard to the F $1s \rightarrow \sigma^*$(C—F) transitions, although precise oscillator strengths cannot be determined on account of overlap, it appears that the ratio of the F $1s \rightarrow \sigma^*$(C—F) peak intensity to the number of fluorines is approximately the same throughout the series (except for *cis*-CHFCHF, which is anomalously weak as noted earlier) and thus the intensity of an individual F $1s \rightarrow \sigma^*$(C—F) transition appears essentially independent of the degree of fluorination. This differs from the systematic increase in the C $1s \rightarrow \sigma^*$(C—F) intensity

TABLE VIII. Comparison of predicted and observed $\sigma^*$ energies.

| | | | $\sigma^*$(C=C) | | | |
|---|---|---|---|---|---|---|
| | | | δ (observed) | | | |
| Species | $R$(C=C)[a] | δ (pred)[b] | $CH_2$ | CHF | $CF_2$ | Avg. |
| $CH_2CH_2$ | 1.339(1) | 11.8 | 10 | | | 10 |
| $CH_2CHF$ | 1.329(6) | 12.4 | 11.2 | | | 11 |
| CHFCHF | 1.324(5) | 12.7 | | (7) | | (7) |
| $CH_2CF_2$ | 1.315(5) | 13.1 | 11.7 | | | 12 |
| $CHFCF_2$ | 1.315(2) | 13.1 | 10 | | | 10 |
| $CF_2CF_2$ | 1.311(2) | 13.3 | | | 13 | 13 |
| 1,3-$C_4F_6$ | 1.488 | 3.7 | | 4.1 | 4.3 | 4.2 |
| | 1.336 | 12.0 | | 9.6 | 7.6 | 8.5 |
| 1,3-$C_4H_6$ | 1.467 | 4.9 | 5.6 | | | 5.6 |
| | 1.344 | 11.5 | 13.6 | | | 13.6 |

| | | | $\sigma^*$(C—F) | | | | | |
|---|---|---|---|---|---|---|---|---|
| | | | | δ (observed) | | | | |
| | | | $CH_2$ | CHF | | $CF_2$ | | |
| Species | $R$(C—F)[a] | δ (pred)[c] | C 1*s* | C 1*s* | F 1*s* | C 1*s* | F 1*s* | Avg. |
| $CH_2CHF$ | 1.347(9) | −2.9 | −2.9 | −3.7 | −2.7 | | | −3.1 |
| CHFCHF | 1.335(5) | −2.4 | | −4.6 | −2.3 | | | −3.5 |
| $CH_2CF_2$ | 1.325(5) | −2.3 | −3.8 | | | −4.1 | −2.2 | −3.4 |
| $CHFCF_2$ | 1.32(3) | −2.1 | | −5.0 | −2.6 | −4.7 | −1.9 | −3.6 |
| $CF_2CF_2$ | 1.319(6) | −2.1 | | | | −4.8 | −2.8 | −3.8 |
| 1,3-$C_4F_6$ | 1.323 | −2.2 | | −2.9 | −1.5 | −3.6 | −2.2 | −2.6 |

[a]From electron diffraction or microwave spectroscopy (Ref. 67).
[b]Based on the correlation line for $Z=12$: $\delta = 84.73 - 54.45\ R$ in angstroms (Ref. 4).
[c]Based on the correlation line for $Z=15$: $\delta = 37.60 - 30.09\ R$ in angstroms (Ref. 4).

with fluorination. We note that the ?-1 and ?-2 transitions clearly are enhanced with fluorination and thus if these features are one-electron transitions to a $\sigma^*$(C—F)-type orbital, this orbital has an appreciably different spatial character than that of the orbital giving rise to the two features below the IP that we have identified as $1s \rightarrow \pi^*$ and $1s \rightarrow \sigma^*$(C—F).

### I. Correlation of $\sigma^*$ energies and bond lengths

The $\sigma^*$ energies relative to the IP ($\delta = -T = E - E_{IP}$) predicted from the molecular geometries and the bond-length correlation[4] are summarized in Table VIII in comparison with the energies of the features assigned to $\sigma^*$(C—F), $\sigma^*$(C—C), and $\sigma^*$(C=C) resonances. In general, there is reasonable agreement between the predicted and observed positions. The worst agreement is found for $1s \rightarrow \sigma^*$(C=C) in *cis*-CHFCHF and 1,4-$C_4F_6$. In the latter species this could be an effect of mixing of the $\sigma^*$(C—C) and $\sigma^*$(C=C) orbitals. A similar phenomenon has been noted in the C 1*s* spectra of several species, particularly cyclic polyatomic molecules.[21,23,50,66] The reasonable agreement between the bond length predicted and observed $\sigma^*$ features in the fluoroethenes suggests that there may be less mixing of the $\sigma^*$(C—F) and $\sigma^*$(C=C) orbitals. This is consistent with the greater energy separation of these orbitals. However, our uncertainty concerning the identity of the strong near-continuum features (those labelled ?-1 and ?-2) precludes more definitive comments.

## VI. SUMMARY

Absolute oscillator strengths in the region of carbon and fluorine *K*-shell excitation of ethene, monofluoroethene, 1,1-difluoroethene, *cis*-1,2-difluoroethene, trifluoroethene, tetrafluoroethene, and 1,3-perfluorobutadiene have been derived from gas-phase energy-loss spectra. Comparisons among the molecules studied showed that fluorination significantly enhances the intensities of C $1s \rightarrow \pi^*$ and C $1s \rightarrow \sigma^*$(C—F) transitions while having little effect on C $1s \rightarrow$Rydberg transitions. In contrast, the C $1s \rightarrow \sigma^*$(C=C) transitions are not particularly enhanced with fluorination suggesting that the $\sigma^*$(C=C) level may lie above the top of the effective potential barrier. A perfluoro effect on the energies of the unoccupied levels was observed, although the $\sigma^*$(C—F) term values are not strongly dependent on the degree of fluorination. The positions of features identified as $\sigma^*$(C—F) and $\sigma^*$(C=C) shape resonances are generally in good agreement with the values predicted from the molecular geometries and the previously reported empirical relationship to bond lengths. Finally, two transitions around 2 and 5 eV above the IP are strongly enhanced with fluorination. These features cannot be assigned satisfactorily as yet.

## ACKNOWLEDGMENTS

This work is supported financially by the Natural Sciences and Engineering Research Council (NSERC) (Canada). One of us (A.P.H.) acknowledges additional support from NSERC and the hospitality of Laboratoire LURE, Orsay where this manuscript was written. We thank Professor H. Baumgartel and Dr. E. Rühl for the loan of the *cis*-CHFCHF sample and Dr. C. E. Brion for providing the high-resolution ISEELS data of $CH_2CHF$ prior to publication.

---

*Present address: Department of Chemistry, University of Alberta, Edmonton, Alberta, Canada.

†Present address: Department of Chemistry, University of British Columbia, Vancouver, British Columbia, Canada.

‡To whom correspondence should be addressed.

[1]C. E. Brion, S. Daviel, R. N. S. Sodhi, and A. P. Hitchcock, *X-Ray and Atomic Inner-Shell Physics, University of Oregon, 1982,* AIP Conf. Proc. No. **94**, edited by Bernd Crasemann (AIP, New York, 1982), p. 426; A. P. Hitchcock, J. Electron Spectrosc. Relat. Phenom. **25**, 245 (1982).

[2]E. E. Koch and B. F. Sonntag, in *Topics in Current Research: Synchrotron Radiation* (Springer, Heidelberg, 1979), p. 269.

[3]J. Stöhr, in *Chemistry and Physics of Solid Surfaces,* edited by R. Vaneslow and R. Howe (Springer, Berlin, 1984), Vol. V, p. 231; J. Stöhr, in *X-Ray Absorption: Principles, Applications, Techniques of EXAFS, SEXAFS and XANES,* edited by D. Konigsberger and R. Prins (Wiley, New York, 1986).

[4]F. Sette, J. Stöhr, and A. P. Hitchcock, J. Chem. Phys. **81**, 4906 (1984).

[5]C. R. Brundle, M. B. Robin, N. A. Kuebler, and H. Basch, J. Am. Chem. Soc. **94**, 1451 (1972); **94**, 1466 (1972).

[6]A. P. Hitchcock, P. Fischer, A. Gedanken, and M. B. Robin, J. Phys. Chem. **91**, 531 (1987).

[7]W. Eberhardt, R. P. Haelbich, M. Iwan, E. E. Koch, and C. Kunz, Chem. Phys. Lett. **40**, 180 (1976).

[8]A. P. Hitchcock and C. E. Brion, J. Electron Spectrosc. **10**, 317 (1977).

[9]M. Tronc, G. C. King, and F. H. Read, J. Phys. B **12**, 137 (1979).

[10]A. Barth, R. J. Buenker, S. D. Peyerhimhoff, and W. Butscher, Chem. Phys. **46**, 149 (1980).

[11]A. P. Hitchcock, S. Beaulieu, T. Steel, J. Stöhr, and F. Sette, J. Chem. Phys. **80**, 3927 (1984).

[12]R. N. S. Sodhi and C. E. Brion, J. Electron Spectrosc. Relat. Phenom. **37**, 1 (1985).

[13]H. O. Beckmann, W. Braun, H. W. Jochims, E. Rühl, and H. Baumgartel, Chem. Phys. Lett. **121**, 499 (1985).

[14]I. Ishii, R. McLaren, A. P. Hitchcock, and M. B. Robin (unpublished).

[15]E. N. Lassettere, in *Chemical Spectroscopy and Photochemistry in the Vacuum-Ultraviolet,* edited by C. Sandorfy, P. J. Ausloos, and M. B. Robin (Reidel, Boston, 1974), p. 43.

[16]M. J. Van der Wiel, Physica **49**, 411 (1970).

[17]R. B. Kay, Ph. E. Van der Leeuw, and M. J. Van der Wiel, J. Phys. B **10**, 2513 (1977).

[18]R. Camilloni, E. Fainelli, G. Petrucelli, and G. Stefani, J.

Phys. B **20**, 1839 (1987).
[19]I. Ishii and A. P. Hitchcock, J. Chem. Phys. **87**, 830 (1987).
[20]J. L. Dehmer, J. Chem. Phys. **56**, 4496 (1972).
[21]D. C. Newbury, I. Ishii, and A. P. Hitchcock, Can. J. Chem. **64**, 1145 (1986).
[22]R. N. S. Sodhi and C. E. Brion, J. Electron Spectrosc. Relat. Phenom. **34**, 363 (1984).
[23]A. P. Hitchcock and I. Ishii, J. Electron Spectrosc. Relat. Phenom. **42**, 11 (1987).
[24]M. Inokuti, Rev. Mod. Phys. **43**, 297 (1971).
[25]M. J. Van der Wiel, in *Photoionization and Other Probes of Many-Electron Interactions,* edited by F. J. Wuilleumier (Plenum, New York, 1976), p. 187.
[26]F. H. Read, J. Phys. (Paris) Colloq. **5**, C1-82 (1978).
[27]G. C. King, M. Tronc, F. H. Read, and R. C. Bradford, J. Phys. B **10**, 2479 (1977).
[28]A. P. Hitchcock and C. E. Brion, Chem. Phys. **33**, 55 (1978).
[29]R. N. S. Sodhi and C. E. Brion, J. Electron Spectrosc. Relat. Phenom. **37**, 97 (1985).
[30]R. D. Leapman, L. A. Grunes, P. J. Fejes, and J. Silcox, *EXAFS Spectroscopy,* edited by B. K. Teo and C. Joy (Plenum, New York, 1981).
[31]G. Doolan and D. Liberman, Phys. Scr. (to be published).
[32]J. L. Dehmer and D. Dill, J. Chem. Phys. **65**, 5327 (1976).
[33]A. P. Hitchcock and C. E. Brion, J. Electron Spectrosc. Relat. Phenom. **18**, 1 (1980).
[34]A. P. Hitchcock and C. E. Brion, J. Electron Spectrosc. Relat. Phenom. **14**, 417 (1978).
[35]A. P. Hitchcock and I. Ishii, Proceedings of EXAFS and Near Edge Structure, Fontevraud, July, 1986 [J. Phys. (Paris) Colloq. **47**, C8-199 (1986)].
[36]A. P. Hitchcock and I. Ishii (unpublished).
[37]H. Petersen, A. Bianconi, F. C. Brown, and R. Z. Bachrach, Chem. Phys. Lett. **58**, 263 (1978).
[38]V. N. Sivkov, V. N. Akimov, A. S. Vinogradov, and T. M. Zimkina, Opt. Spektrosk. **57**, 265 (1984) [Opt. Spectrosc. (USSR) **57**, 160 (1984)].
[39]C. M. Truesdale, D. W. Lindle, P. H. Kobrin, U. E. Becker, H. G. Kerkhoff, P. A. Heimann, T. A. Ferrett, and D. A. Shirley, J. Chem. Phys. **80**, 2319 (1984).
[40]D. M. Barrus, R. L. Blake, A. J. Burek, K. C. Chambers, and A. L. Pregenzer, Phys. Rev. A **20**, 1045 (1979).
[41]F. C. Brown, R. Z. Bachrach, and A. Bianconi, Chem. Phys. Lett. **54**, 425 (1978).
[42]I. Ishii, R. McLaren, A. P. Hitchcock, M. B. Robin, and K. D. Jordan (unpublished).
[43]V. N. Sivkov, V. N. Akimov, A. S. Vinogradov, and T. M. Zimkina, Opt. Spektrosk. **60**, 318 (1986) [Opt. Spectrosc. (USSR) **60**, 194 (1986)].
[44]The splittings between the C $1s\sigma_g$ and C $1s\sigma_u$ in $C_2H_4$ and $C_2F_4$ are expected to be less than 0.1 eV [Ref. 10 and W. Butscher, R. J. Bunker, and S. D. Peyerimhoff, Chem. Phys. Lett. **52**, 449 (1977)]. This is insignificant relative to our limited resolution (0.6 eV), and probably not detectable even with high resolution[9] because of natural linewidth limitations.
[45]W. L. Jolly, K. O. Bomben, and C. J. Eyermann, At. Data Nucl. Data Tables **31**, 433 (1984).
[46]D. Arvantis, U. Döbler, L. Wenzel, K. Baberschke, and J. Stöhr, Surf. Sci. **178**, 687 (1986).
[47]D. Arvantis, K. Baberschke, L. Wenzel, and U. Döbler, Phys. Rev. Lett. **57**, 3175 (1986).
[48]A. P. Hitchcock and C. E. Brion, J. Electron Spectrosc. Relat. Phenom. **13**, 193 (1978); **18**, 139 (1979).
[49]W. H. E. Schwarz, U. Seeger, and R. Seeger, Chem. Phys. (to be published).
[50]J. A. Horsley, J. Stöhr, A. P. Hitchcock, D. C. Newbury, A. L. Johnson, and F. Sette, J. Chem. Phys. **83**, 6099 (1985).
[51]V. N. Akimov, A. S. Vinogradov, A. A. Pavlychev, and V. N. Sikov, Opt. Spektrosk. **59**, 342 (1985) [Opt. Spectrosc. **59**, 206 (1985)].
[52]M. N. Paddon-Row, N. A. Rondan, K. N. Houk, and K. D. Jordan, J. Am. Chem. Soc. **104**, 1143 (1982).
[53]K. H. Sze, C. E. Brion and A. Katrib (unpublished).
[54]H. Baumgartel and E. Rühl (private communication).
[55]W. Eberhardt, T. K. Sham, R. Carr, S. Krumacher, M. Strongin, S. L. Wergand, and D. Wesner, Phys. Rev. Lett. **50**, 1038 (1983).
[56]K. Müller-Dethlefs, M. Sander, L. A. Chewter, and E. W. Schlag, J. Phys. Chem. **88**, 6098 (1984).
[57]C. H. Chang, A. L. Andressen, and S. H. Bauer, J. Org. Chem. **36**, 920 (1971).
[58]C. R. Brundle and M. B. Robin, J. Am. Chem. Soc. **92**, 5550 (1970).
[59]K. Kuchistu, T. Fukuyama, and Y. Morino, J. Mol. Struct. **4**, 41 (1969).
[60]E. Lindholm, J. Chem. Phys. **85**, 1484 (1986).
[61]P. D. Burrow and K. D. Jordan, Chem. Phys. Lett. **36**, 594 (1979).
[62]I. Sauers, L. G. Christophorou, and J. G. Carter, J. Chem. Phys. **71**, 3016 (1979).
[63]D. A. Dixon, J. Phys. Chem. **90**, 2038 (1986).
[64]N. S. Chieu, P. D. Barrow, and K. D. Jordan, Chem. Phys. Lett. **68**, 121 (1978).
[65]A. P. Hitchcock, P. Fischer, and R. McLaren, in *Giant Resonances in Atoms, Molecules and Solids,* Proceedings of the NATO Advanced Study Institute, Les Houches, France, 1986 (Plenum, New York, in press).
[66]A. P. Hitchcock, D. C. Newbury, I. Ishii, J. Stöhr, A. L. Johnson, R. D. Redwing, and J. A. Horsley, J. Chem. Phys. **85**, 4849 (1986).
[67]*Structure Data of Free Polyatomic Molecules,* Vol. 7 of Landolt-Börnstein, New Series II, edited by K. H. Hallwege (Springer, Berlin, 1976).